2005:50

LICENTIATE THESIS

L

Mathematical Modeling of Electromagnetic Disturbances in Railway System

Farid Monsefi

Luleå University of Technology
Department of Computer Science and Electrical Engineering
Division of EISLAB
Department of Civil and Environmental Engineering
Division of Operation and Maintenance Engineering

2006:50 | ISSN: 1402-1757 | ISRN: LTU-LIC -- 06/50 -- SE

Mathematical Modeling of Electromagnetic Disturbances in Railway System

Farid Monsefi

EISLAB
Department of Computer Science and Electrical Engineering
Division of Operation and Maintenance Engineering
Luleå University of Technology
Luleå, Sweden

Supervisors:

Jerker Delsing
Uday Kumar

To my family

Abstract

By introduction of modern electronics into railway system, new challenges in understanding the electric and electromagnetic behavior of these systems arise. In this thesis, electromagnetic modeling of electrical networks above dielectric and perfect electrically conducting surfaces are studied. The approach is based on the Partial Element Equivalent Circuit (PEEC) method for solving Maxwell's equations.

The most challenging problem within electromagnetic modeling of large systems is computational speed and for railway systems, modeling of the ground becomes the major bottleneck. The purpose of the thesis is to develop maintenance program for the railway system in the Northern Sweden to deal with the failures created by electromagnetic disturbances using mathematical modeling of the electromagnetic phenomena. First, a grid PEEC approach was used to improve the computation time of the original program. This approach utilizes an algorithm to distribute the calculations on computers in a local area network. It was shown that the computation time for large systems could be improved in some stages of the computation process.

The second approach to improve the computational efficiency of the PEEC method utilized the theory of complex images. This results in an appropriate mathematical tool to study and describe the generated electric fields above the earth, as a dielectric- or perfectly electric conducting surface. Different mathematical models were applied to analyze and plot the current distribution on structures and the electric field generated by several structures above a perfect electrical conducting surface. The tests were verified by analytical methods and the traditional PEEC computation method. In the traditional PEEC method, the numerical solution of mathematical modeling of the ground did form the major effort due to the large number of unknown variables in the corresponding linear equation system. By using of the complex image methods, where the effect of the ground was approximated, the computational time was clearly improved in the case studies. This combination of the PEEC method and the method of complex images resulted in an ultimate linear equation system by a smaller number of unknown variables and therefore a considerable improvement of the computational time.

By use of electromagnetic modeling, it will be possible to study the disturbances due to transients and discharges, and also to expand the data bases for artificial intelligence. Defining the problem and determining what can be obtained by using of computational electromagnetic modeling, will be a step towards developing a more appropriate maintenance program for the railway system in the northern Sweden.

Contents

Preface

This thesis is consisted of my research and contributions within electromagnetic simulations and modeling using the PEEC method. Electromagnetic analysis in this work, has been to develop methods which can be applied to improvement of the maintenance actions within railway system in northern Sweden. My research has jointly been supported by EISLAB and Division of Operation and Maintenance Engineering, Luleå University of Technology.

I would like to thank my supervisors, Prof. Jerker Delsing and Prof. Uday Kumar, for their effectual supervision, steady support and valuable comments in the course of the thesis. I am grateful to Dr. Jonas Ekman, for his inspiring encouragement and illuminating comments and instructions to all the work my thesis is based on.

I would like to thank my friends and colleagues at Computer Science and Electrical Engineering and The Division of Operation and Maintenance Engineering in Luleå University of Technology. I would also like to thank Mr. Aditya Parida for his help and friendship.

Finally, I wish to express my gratitude to my family for their unconditional support during my work on the thesis.

Part I

Chapter 1

Thesis Introduction

This chapter introduces Reliability-centered maintenance (RCM) and EMC-related maintenance of the railway system. The theoretical background of electromagnetic modeling techniques is also discussed in which the complexity of the applied mathematical tools and the numerical solution of the associated models are concisely discussed.

1.1 Thesis Introduction

During the past twenty years, the concept of maintenance has been changing more than other management discipline, possibly due to a huge increase in the number and variety of physical assets, i.e. equipment and plant. To ensure the right maintenance at the right time to sustain system functions, one may apply reliability-centered maintenance (RCM). This discipline is a very useful tool in different industries and can be adapted to particular constraints and requirements of the industry where it is applied. Analysis of risk and simulations may be used when carrying out the computerized tool concerning implementation of RCM. Electromagnetic compatibility (EMC) tests and modeling are functioning as an indicator when maintaining the electrified railway networks and systems. There are standard methods in railway applications for reducing disturbance of the feeding arrangements and feeder networks which can cause disturbance to electrical/electronic systems. Some of feeder networks can even cause direct danger to life. These will be discussed in the following chapters where the electromagnetic compatibility (EMC) is a major issue within European railway standards.

In order to guarantee operability of advanced railway signaling and vehicles, EMC tests may be compared to results from electromagnetic modeling. The experimental techniques are expensive and time consuming but are still widely used. Hence, the advantage of obtaining data from tests can be weighted against the large amount of time and expense required to operate such tests. Analytic solution of Maxwell's equations offers many advantages over experimental methods but applicability of analytical electromagnetic modeling is often limited to simple geometries and boundary conditions. The analytic solution of Maxwell's equations by the methods of *Separation of variables*

and *Series expansions* are not applicable in a general case and in a real-world application, these analytic solutions are of a very limited scope. Availability of high performance computers during the last decades has been one of the reasons to use numerical techniques within electromagnetic modeling to solve Maxwell's equations for complicated geometries and boundaries.

The goal of this work is to improve the maintenance program for the railway system in the northern Sweden. To deal with the failures created by electromagnetic disturbances, mathematical modeling of the electromagnetic phenomena is applied. It will be shown that the calculation time for large systems, resembling railways, could be improved in some stages of the computation process. The most challenging problem within electromagnetic modeling of large systems is computational speed and for railway systems, modeling of the ground becomes the major bottleneck. It is shown that how applying the PEEC methodology in combination with complex image methods and parallel algorithms can improve the solution of the electromagnetic field modeling.

The main focus in this work has been on computational speed ups for EM problems containing large ground planes. In this context, some tests were verified by analytical methods and the traditional PEEC computation method. In the traditional PEEC method, the numerical solution of mathematical modeling of the ground constituted the major effort due to the large number of unknown variables in the corresponding linear equation system. By using of the complex image methods (CIM), where the effect of the ground is approximated, the computational time will be clearly reduced in the case studies. It will also be shown that the combination of the PEEC method and the method of complex images results into an ultimate linear equation system by a smaller number of unknown variables and therefore a considerable reduction of the computational time.

1.2 Numerical PEEC method and Dyadic Green's Function

The most popular numerical techniques are (1) Finite difference methods, (2) Finite element methods, (3) The method of moments, and (4) The partial element equivalent circuit (PEEC) method. The first three methods will briefly be presented in the following chapters. The fourth technique, the PEEC method is presented in Chapter 4 where *Grid-PEEC*, as a parallel algorithm, is discussed for numerically large systems. The differences in the numerical techniques have its origin in the basic mathematical approach and therefore make one technique more suitable for a specific *class of problem* compared to the others.

The electromagnetic modeling of computationally large systems like railways involves challenges in form of abnormal simulation time for computers using numerical algorithms. As an approach to perform the computational time, the parallel algorithm of *Grid-PEEC* is applied which is based on a traditional PEEC algorithm. A general feature of this parallel algorithm is that the computational time is constantly dependent on the number of computers which are solving the integral form of Maxwell's equations, discretized by

the traditional PEEC method. However, a certain improvement of the calculation time, especially when calculating partial elements, was experienced. This improvement was, in all of the possible options, a result of the trade-off between the number of the parallel computers and memory consuming for every individual computer; the fewer number of computers, the shorter elapsed time for communication among them and vice versa. This is actually a general feature of parallel computing.

It will be shown that how the method of complex images can be combined with the PEEC method to reduce this computational time. Combination of these methods leads into solving an equivalent problem where the time-consuming calculation of the ground effects is approximated. The mathematical background of the method of images is discussed in the following chapters. Further, it will be shown that how this method can be applied to derive mathematical models for both small and large systems above a perfectly electric conducting (PEC) surface, resembling the railway system. Combination of the PEEC method and the method of complex images results into a considerable improvement in the calculation time. In the complex image applications, an important stage is to determine the associated dyadic Green's function by appropriate numerical methods; solving the integral form of the Maxwell's equations, by this dyadic Green's function as a part of the integrand, is the another crucial issue within computational electromagnetism. Application of the method of complex images and the PEEC method, involving different scattering structures above a PEC surface, results into a remarkably reduced computational time.

1.3 Computational Electromagnetics for Layered Media

Determining of Green's functions for stratified media has, during the last decades, been an important and fundamental stage to design of high-frequency circuits. In the case of a layered medium, a so-called *mixed-potential integral equation (MPIE)*, is applied to the associated geometry [1]. MPIE can be solved in both spectral- and spatial- domain and the both solutions require appropriate Green's functions. The Green's functions for multi-layered planar media are represented by the Sommerfeld integral whose integrand is consisted of the Hankel function, and the closed-form spectral-domain Green's functions [2]. A two-dimensional inverse Fourier transformation is needed to determine the spectral-domain Green's functions analytically via the following integral which is along the Sommerfeld integration path (SIP) and k_ρ-plane as

$$G = \frac{1}{4\pi} \int_{SIP} dk_\rho k_\rho H_0^{(2)}(k_\rho \rho) \tilde{G}(k_\rho) \tag{1.1}$$

where $H_0^{(2)}$ is the Hankel function of the second kind; G and $\tilde{G}$ are the Green's functions in the spatial- and spectral- domain. One of the topics in this context is that there is no generally analytic solution to the Hankel transform of the closed-form spectral-domain

Green's function. Numerical solution of the above transformation integral is very time-consuming, partly due to the slow-decaying Green's function in the spectral domain, partly due to the oscillatory nature of the Hankel function. Dealing with such problem constitutes one of the major topics within the computational electromagnetics for multi-layered media. In many applications, the *Discrete complex image methods* (DCIM) is used to handle this numerically time-consuming process. The strategy in this process is to obtain Green's functions in closed form as

$$G \cong \sum_{k=1}^{N} a_n \frac{e^{-jkr_m}}{r_m} \tag{1.2}$$

where

$$r_m = \sqrt{\rho^2 - b_m^2} \tag{1.3}$$

with $j = \sqrt{-1}$ will be complex-valued. The constants a_n and b_m are to be determined by numerical processes such Prony's method [3][4]. In dyadic form and by assuming an $e^{j\omega t}$ time dependence, the electric field at an observation point $\vec{r}$ produced by a surface current $\vec{J}$ of a surface S' can be expressed as

$$\begin{aligned} \mathbf{E}(\mathbf{r}) &= -j\omega \int_{S'} \left[\overline{\overline{I}} + \frac{1}{\beta^2 \nabla\nabla} \right] \frac{\mu e^{-j\beta R}}{4\pi R} \mathbf{J}(\mathbf{r}, \mathbf{r}') dS' \\ &= \int_{S'} \mathbf{G}(\mathbf{r}, \mathbf{r}') \mathbf{J}(\mathbf{r}, \mathbf{r}' dS' \end{aligned} \tag{1.4}$$

where $\beta = \omega\sqrt{\mu\epsilon}$ by μ and ϵ as the electromagnetic characteristics for the layered medium; R is the distance from the source point to the field point. $\overline{\overline{I}}$ is the unit dyad and $\mathbf{G}(\mathbf{r}, \mathbf{r}')$ is defined as the dyadic Green's function.

There are different methods to construct the auxiliary Green's function in the case of boundary value problems which are as a consequence of using mathematics to study problems arising in the real world. Within EMC, Green's function is applied to convert a partial differential equation to an integral equation. The numerical solution of an integral equation has the general property that the coefficient matrix in the ultimate linear equation $Ax = y$ will consist of a dense coefficient matrix A and a relatively fewer number of elements in the unknown vector x. Numerical solution of a general integral equation involves challenges due to the ill-conditioned coefficient matrix A, as a rule and not as an exception; the integration operator is a smoothing operator and determining the kernel of an integral equation will be the opposite operator. This is the main reason of the ill-conditioning. Generally and depending on the kind of problem, there are several numerical methods to get rid of this ill-conditioning and in the case of solution of Maxwell's equations by the integral-based PEEC method, ill-conditioning will be a problem to handle.

Chapter 2

Reliability-Centered Maintenance (RCM) and Railway system

In this chapter, the concept of Reliability-Centered Maintenance (RCM) is presented. The related concept of Failure Mode and Effect Analysis (FMEA), followed by a short introduction to EMC-related European standards and measurements within railway system are also presented.

2.1 Reliability-Centered Maintenance

RCM was initially developed for the commercial aviation industry in the late 1960s and the result was published as a document which was called MSG-3. This standard did constitute an accepted methodology that has been applied in a wide range of industries. RCM achieves effectively the required safety and availability levels of equipment and structures. The result is intended to be improved overall safety, availability, and economy of operation. For establishing a preventive maintenance program, the application of RCM requires a detailed analysis of the product and its functions. A maintenance program is the set of tasks resulted from the RCM analysis where the maintenance objectives are:

- To maintain the function and inherent safety and reliability levels
- Optimization of availability
- Monitoring the condition of specific safety, and critical- and costly- components
- Obtaining the necessary information for design improvement
- Accomplishing these goals at a minimum total life cycle cost (LCC)

The present industrial competition is global and forms a fragmented international market with customers expecting to get the best product with the best price. Success in manufacturing, and indeed survival, is increasingly more difficult to ensure and it requires continuous development and improvement of the way products are produced. Meeting customer demands requires a high degree of flexibility, low-cost/low-volume manufacturing skills, and short delivery times. These demands make manufacturing performance a strategic weapon for competition and future success. Many managers believe that the greatest potential for improvement of competitiveness lies in better production management. Productivity, in its turn, is a key weapon for manufacturing companies to stay competitive in a continuous growing global market. Increased productivity can be achieved through increased availability. This has directed focus on different maintenance strategies. Increased availability through efficient maintenance can be achieved through less corrective maintenance actions and more accurate preventive maintenance intervals.

2.2 Failure Mode and Effect Analysis (FMEA)

FMEA is defined as the work procedure concerning different phases of production development and to prepare for identifying potential failure occurrence. FMEA prepares also for quality performance and it is applied by people who are working with production development by a high degree of competition where reliability and high quality are respectively desired. FMEA work is combined in the production development in a well-planned and schematic way where the analysis is growing successively and it is deepened tactfully with a detailed development process. A well-done FMEA is also functioning as a valuable documentation which will be used as a reference in the future when, for instance, it is time for a new analysis. FMEA is applied within different fields such [5]

- *Product planning*, in which risk assessment is introduced based on desired functions of the product. To identify the costumer's requirement and to guarantee that the development efforts is directed against the fields that are important for the costumer, one should apply the method of Quality Function Development (QFD). This method identifies the costumer's requirement and interpret it in technical terms.

- *Product development*, as a process where the product is assessed and discussed if it is, among others, as faultless as possible.

- *Production preparing*, applied to guarantee a well-functioning production process, i.e. a process where availability, security, and capability are respectively required.

- *Material acquisition*, in which the detailed components are considered in their entirety; highly estimated risk, which may affect the choice of components, is also considered.

- *Production installation*, which must be focused on the requirements due to the manufactured functions such accuracy, production discretion, maintenance requirement, operation security etc.

- *Production*, in which the analysis of failure effect is included where identifying the possibility of failure occurrence is the focus of interest.

The basic principle is that the product- and process- changing will be analyzed within FMEA. Sometimes it is necessary to prioritize and make a selection of actions that considers the usefulness of them which is mentioned and expected in the analysis. The order of priority is based on:

- concepts concerning both personal- and product- safety

- already known problem fields

- large economical consequences

The method of FMEA is especially appropriate for serial, functional systems and processes where every detailed component or process is acting together in a chain of events; if a link is out of order, the whole system will be stopped, unlike a so-called redundant system where several parallel sub-systems are functioning independent from each other. FMEA may be applied to different levels and different moments; the longer a project is, the more detailed FMEA is. An analysis will be made firstly for a comprehensive level, then for each sub-system, and finally for lowest level, i.e. the component level. The choice of the analysis level occurs after studying the object which is illustrated in flow charts.

2.3 EMC Standards and Railway System

The aim of the common EMC laboratory tests is to demonstrate that equipment will operate satisfactory in its electromagnetic environment, and the equipment does not affect another equipment. The principle is that these tests must be realistic, realizable, and repeatable and they have to simulate real-world conditions where requirements of standards and contracts are met. Within the standards, different railway issues are first addressed for a particular problem and then maximum radiated emissions will be measured after placing the equipment under test (EUT) on an open area test site (OATS) with an antenna placed 10 m from it [6]. EMC tests are designed within railway system to ensure the above mentioned principle. Depending on the particular problem, two major test groups are implemented [7]. These are:

- *Emissions tests*, in which the equipment under test does not affect the operation of other equipment; implemented to protect radiocommunications services.

- *Immunity tests* to ensure that the equipment under test operates satisfactory on the environments close to, for instance, heavy machinery and transmitters.

These test groups are sub-divided into several test categories such as conducted or radiated, and also frequency domain (continuous) or time domain. The categorization is intended to realize the most appropriate and effective test method matching the dominant coupling mechanism. As an example for EMC tests simulating induced pulses from nearby lightning strikes, it will be an appropriate choice to implement time domain test due to the time-domain nature of a lightning strike; frequency measurements are however applied when EMC tests simulating interference from frequency-domain radio transmitters. In European countries, the EN 50121 series [8] of standards has recently been established according to which rail manufacturers across Europe have agreed levels of emission and immunity at radio frequencies so that modern electric locomotives have nowadays significant emissions in the low frequencies between 9 kHz and 100 kHz. The methods are not suitable for solving disturbances problems on operational railways owing to be adapted, originally, for stationary equipment [7].

In traditional railway EMC measurements, voltage due to the induced longitudinal voltage (VL) on line-side cabling, was measured continuously as the train moved along the affected part of the line; exceeding the permissible limit for VL, increases the risk of electric shock for staff and also a higher probability of equipment malfunction and failure. To enable freetrade for European manufacturers of railway equipment and to comply with the EMC directive, the EN50121 set of product specific EMC standards is applied. The standards which cover different areas of interest within different sectors of the railway industry are harmonized which means that all European countries use them. These six standards are as follows.

- *EN* $50121 - 1$. This standard considers a general point of view regarding EMC measurements.

- *EN* 50121 − 2. Based on measurements all over Europe, a limit is set regarding emissions of existing railway stock in different train speeds. This type of standard covers emission of the whole railway system to the outside world.
- *EN* 50121 − 3 − 1. It considers rolling stock related to train and completed vehicle. Like EN 50121 − 2, this standard uses the same test method but with the train operating at different speeds. In this way, results from one test may not satisfy the requirements of the other standard.
- *EN* 50121 − 3 − 2. This standard deals with rolling stock related to apparatus. In the case of a multi-port apparatus, all types of port has to be tested. Special aspects of emission limits and immunity are considered.
- *EN* 50121 − 4. This standard is applied to signaling and telecommunication apparatus installed in railway environment. It deals actually with emission and immunity of the signaling and telecommunications apparatus.
- *EN* 50121 − 5. It deals with emission and immunity of fixed power supply installations and apparatus. There are limits for both immunity levels and emissions for the power supply system.

To cover the frequency range of 9 kHz and 30 MHz, the use of at least one loop antenna is suggested by the standard. For electric field measurement, i.e. above 30 MHz, a biconical antenna is used but the advanced antenna design may cover the whole range by one bi-log antenna. Nowadays, an spectrum analyzer can sweep the set frequency range in less than 0.2 seconds for capturing continuous emissions from the passing train. For different purposes, different train passes are required. As an example, EN 50121 − 2 requires at least three train passes to the electric antenna as a part of a moving test whilst the slow moving test of EN 50121 − 3 − 1 requires at least nine train passes. By aid of a special arrangement, the problem of requiring nine train passes will however be performed by doing a single EN 50121 test. This method utilizes simultaneously running analyzers and a control computer which is downloading each spectrum [7].

Chapter 3

Mathematical Tools in Electromagnetism

The mathematical tools applied to solution of radiated electromagnetic fields are presented in this chapter. Application of these mathematical tools to structures which are close to- and within- dielectrics and perfectly electric conducting materials is also presented.

3.1 Basic Concepts in Electromagnetism

In constructing the electrostatic model an electric field intensity vector **E** and an electric flux density vector, **D**, are respectively defined. The fundamental governing differential equations are [9]

$$\begin{aligned} \nabla \times \mathbf{E} &= 0 \\ \nabla \cdot \mathbf{D} &= \rho_v \end{aligned} \tag{3.1}$$

where ρ_v is volume charge density and ϵ is dielectric constant. For linear and isotropic media, **E** and **D** are related by relation

$$\mathbf{D} = \epsilon \mathbf{E} \tag{3.2}$$

The fundamental governing equations for magnetostatic model are

$$\begin{aligned} \nabla \cdot \mathbf{B} &= 0 \\ \nabla \times \mathbf{H} &= \mathbf{J} \end{aligned} \tag{3.3}$$

where **B** and **H** are defined as magnetic flux density vector and magnetic field intensity vector respectively. **B** and **H** are related as

$$\mathbf{H} = \frac{1}{\mu_0 \mu_r} \mathbf{B} \tag{3.4}$$

where μ is defined as magnetic permeability of the medium which is measured in H/m. The medium in question is assumed to be linear and isotropic. Eqs. (3.1) and (3.3) are known as Maxwell's equations and form the foundation of electromagnetic theory. As it is seen in the above relations, **E** and **D** in the electrostatic model are not related to **B** and **H** in the magnetostatic model. The coexistence of static electric fields and magnetic electric fields in a conducting medium causes an electromagnetostatic field and a time-varying magnetic field gives rise to an electric field. These are verified by numerous experiments. Static models are not suitable for explaining time-varying electromagnetic phenomenon. Under time-varying conditions it is necessary to construct an electromagnetic model in which the electric field vectors **E** and **D** are related to the magnetic field vectors **B** and **H**. In such situations, the equivalent equations are constructed as

$$\nabla \times \mathbf{E} = -\frac{\partial \mathbf{B}}{\partial t} \tag{3.5}$$

$$\nabla \times \mathbf{H} = \mathbf{J} \tag{3.6}$$

$$\nabla \cdot \mathbf{D} = \rho_v \tag{3.7}$$

$$\nabla \cdot \mathbf{B} = 0 \tag{3.8}$$

where **J** is current density. As it is seen, the Maxwell's equations above are in differential form. To explain electromagnetic phenomena in a physical environment, it is more

convenient to convert the differential forms into their integral-form equivalents. There are several techniques to convert differential equations into integral equations but in the above cases, one may apply Stokes's theorem to obtain integral form of Maxwell's equations after tasking the surface integral of both sides of the equations over an open surface S with contour C. The result will be constructed as in the following table.

Maxwell's equations

Differential form	*Integral form*	
$\nabla \times \mathbf{H} = \mathbf{J} + \frac{\partial \mathbf{D}}{\partial t}$	$\oint_C \mathbf{H} \cdot d\mathbf{L} = I + \int_S \frac{\partial \mathbf{D}}{\partial t} \cdot d\mathbf{S}$	(3.9)
$\nabla \times \mathbf{E} = -\frac{\partial \mathbf{B}}{\partial t}$	$\oint_C \mathbf{E} \cdot d\mathbf{L} = \int_S \frac{\partial \mathbf{B}}{\partial t} \cdot d\mathbf{S}$	(3.10)
$\nabla \cdot \mathbf{D} = \rho_v$	$\int_S \mathbf{D} \cdot d\mathbf{S} = \int_V \rho_v dV$	(3.11)
$\nabla \cdot \mathbf{B} = 0$	$\int_S \mathbf{B} \cdot d\mathbf{S} = 0$	(3.12)

ρ_v, in the above table, is the electric charge density in C/m^3. The PEEC method uses the integral form of the Maxwell's equations to solve the electromagnetic field quantities and also the partial elements.

3.2 Green's Functions

When a physical system is subject to some external disturbance, a non-homogeneity arises in the mathematical formulation of the problem, either in the differential equation or in the auxiliary conditions or both. When the differential equation is nonhomogeneous, a particular solution of the equation can be found by applying either the method of undetermined coefficients or the variation of parameter technique. In general, however, such techniques lead to a particular solution that has no special physical significance. Green's functions[1] are specific functions that develop general solution formulas for solving nonhomogeneous differential equations. Importantly, this type of formulation gives an increased physical knowledge since every Green's function has a physical significance. This function measures the response of a system due to a point source somewhere on the fundamental domain, and all other solutions due to different source terms are found to be superpositions [2] of the Green's function. There are, however, cases where Green's

[1] George Green, 1793-1841, was one of the most remarkable of nineteenth century physicists, a self-taught mathematician whose work has contributed greatly to modern physics.

[2] Consider a set of functions ϕ_n for $n = 1, 2, ..., N$. If each number of the functions ϕ_n is a solution to the partial differential equation $L\phi = 0$, with L as a linear operator and with some prescribed boundary conditions, then the linear combination $\phi_N = \phi_0 + \sum_{n=1}^{N} a_n \phi_n$ also satisfies $L\phi = g$. Here, g is a known excitation or source. This fundamental concept is verified in different mathematical literature.

functions fail to exist, depending on boundaries. Although Green's first interest was in electrostatics, Green's mathematics is nearly all devised to solve general physical problems . The inverse-square law had recently been established experimentally, and George Green wanted to calculate how this determined the distribution of charge on the surfaces of conductors. He made great use of the electrical potential and gave it that name. Actually, one of the theorems that he proved in this context became famous and is nowadays known as Green's theorem. It relates the properties of mathematical functions at the surfaces of a closed volume to other properties inside. The powerful method of Green's functions involves what are now called Green's functions, $G(x, x\prime)$. Applying Green's function method, solution of the differential equation $Ly = F(x)$, by L as a linear differential operator, can be written as

$$y(x) = \int_0^x G(x, x\prime)F(x\prime)dx\prime \tag{3.13}$$

To see this, consider the equation

$$\frac{dy}{dx} + ky = F(x)$$

which can be solved by the standard integrating factor technique to give

$$y = e^{-kx} \int_0^x e^{kx\prime} dx\prime = \int_0^x e^{-k(x-x\prime)} F(x\prime)dx\prime$$

so that $G(x, x\prime) = e^{-k(x-x\prime)}$. This technique may be applied to other more complicated systems. In an electrical circuit the Green's function is the current due to an applied voltage pulse. In electrostatics, the Green's function is the potential due to a change applied at a particular point in space. In general the Green's function is, as mentioned earlier, the response of a system to a stimulus applied at a particular point in space or time. This concept has been readily adapted to quantum physics where the applied stimulus is the injection of a quantum of energy. It is in the quantum domain that the application of Green's functions to physical problems has grown most spectacularly in the past few decades.

Within electromagnetic computation, it is common practice to use two methods for determining the Green's function in the cases where there is some kind of symmetry in the geometry of the electromagnetic problem. These are the eigenvalue formulation and the method of images. These two methods are described in the following sections, but in order to its importance, the method of the eigenfunction expansion method is first presented.

3.3 Eigenfunction Expansion Method

The method of eigenfunction expansion can be applied to derive the Green's function for partial differential equations by known homogeneous solution. The partial differential

equation

$$\begin{aligned} U_{xx} &= \frac{1}{\kappa}U_t + Q(x,t), && 0 < x < L, t > 0 \\ B.C. &: U(0,t) = 0, U(L,t) = 0, && t > 0 \\ I.C. &: U(x,0) = F(x), && 0 < x < L \end{aligned} \tag{3.14}$$

with

$$\begin{aligned} Q(x,t) &= \frac{1}{\kappa}K_t(x,t) - q(x,t) \\ F(x) &= f(x) - K(x,0) \end{aligned} \tag{3.15}$$

features a problem with homogeneous boundary conditions. The Green's function, in this case, can be represented in terms of a series of orthonormal functions that satisfy the prescribed boundary conditions. In this process, it is assumed that the solution of the partial differential equation may be written in the form [10]

$$U(x,t) = \sum_{n=1}^{\infty} E_n(t)\Psi_n(x) \tag{3.16}$$

where $\Psi_n(x)$ are eigenfunctions belonging to the associated eigenvalue problem[3]

$$X'' + \lambda X = 0 \tag{3.17}$$

by prescribed boundary condition (B.C.) and initial conditions (I.C.). $E_n(t)$ are time-dependent coefficients to be determined. It is also assumed that termwise differentiation is permitted[4]. In this case

$$U_t(x,t) = \sum_{n=1}^{\infty} E_n'(t)\Psi_n(x) \tag{3.18}$$

and

$$U_{xx}(x,t) = \sum_{n=1}^{\infty} E_n(t)\Psi_n''(x)$$

which together with (3.17) gives

$$U_{xx}(x,t) = -\sum_{n=1}^{\infty} \lambda_n E_n(t)\Psi_n(x) \tag{3.19}$$

[3]Clearly $U(x,t)$, satisfies the prescribed homogeneous boundary conditions, since each eigenfunction $\Psi_n(x)$ does.

[4]The operation of termwise differentiation of an infinite series is valid according to: Corollary If $f_k(x)$ has a continuous derivative on $[a,b]$ for each $k = 1,2,3,...$ and if $\sum_{k=1}^{\infty} f_k(x)$ converges to $S(x)$ on $[a,b]$ and if the series $\sum_{k=1}^{\infty} f_k'(x)$ converges uniformly to $g(x)$ on $[a,b]$ then $S'(x) = g(x)$ for every $x \in [a,b]$; equivalently $\frac{d}{dx}\sum_{k=1}^{\infty} f_k(x) = \sum_{k=1}^{\infty} \frac{d}{dx} f_k(x)$...". Introduction to Mathematical Analysis page 206-William Parzynski, Philip W. Zipse.

This is a result of applying the superposition principle which can be deduced as $\Psi_n''(x) = -\lambda_n \Psi_n(x)$ from (3.17). Next, by rewriting the partial differential equation above as

$$\kappa U_{xx} = U_t + \kappa Q(x,t) \tag{3.20}$$

and inserting the expressions (3.18) and (3.19) into the right-hand side of (3.19), it can be obtained that

$$\kappa U_{xx} = \sum_{n=1}^{\infty} [E_n'(t) + \kappa \lambda_n E_n(t)] \Psi_n(x) \tag{3.21}$$

The right-hand side of equation above is interpreted as a generalized Fourier series[5] of the function κU_{xx} for a fixed value of t. Thus, the Fourier coefficients are defined as

$$\begin{aligned} E_n'(t) + \kappa \lambda_n E_n(t) &= \kappa \frac{1}{\|\Psi_n(x)\|^2} \int_0^L Q(x,t) \Psi_n(x) dx \\ \text{for } \; n &= 1, 2, ... \end{aligned} \tag{3.22}$$

where $\|\Psi_n(x)\|$ is defined as the norm of $\Psi_n(x)$ with the relation

$$\|\Psi_n(x)\|^2 = \int_0^L [\Psi_n(x)]^2 dx, \text{ for } n = 1, 2, ... \tag{3.23}$$

Eq. (3.21) as a first-order linear differential equation, has the general solution

$$E_n(t) = \left(c_n + \frac{1}{\kappa} \int_0^t exp(\frac{1}{\kappa} \lambda_n) P_n(\tau) d\tau \right) exp(-\frac{1}{\kappa} \lambda_n t) \tag{3.24}$$

for $n = 1, 2, 3, ...$ by the assumption that $\lambda_n \neq 0$ for all n. It has to be added that c_n are arbitrary constants. In the equation above, $P_n(t)$ is defined as

$$P_n(t) = \frac{1}{\|\Psi_n(x)\|^2} \int_0^L Q(x,t) \Psi_n(x) dx, \text{ for } n = 1, 2, 3, ... \tag{3.25}$$

Now, by substituting (3.24) into (3.16), it will be obtained that

$$U(x,t) = \sum_{n=1}^{\infty} \left(c_n + \frac{1}{\kappa} \int_0^t exp(\frac{1}{\kappa} \lambda_n) P_n(\tau) d\tau \right) exp(-\frac{1}{\kappa} \lambda_n t) \Psi_n(x) \tag{3.26}$$

[5]These series can be used in developing infinite series like Fourier series and have the general form $f(x) = \sum_{n=1}^{\infty} c_n U_n(x)$ for $x_1 < x < x_2$, where the set of functions $\{U_n(x)\}$ is orthogonal on the specified interval by a given weighting function $w(x) > 0$, that is $\int_{x_1}^{x_2} U_n(x) U_n(x) w(x) dx = 0$, for all $k \neq n$.

For determining the arbitrary coefficients c_n, $n = 1, 2, 3, ...$, one shall force equation 3.25 to satisfy the prescribed initial condition. By using the above process and applying the method of moments (MoM), described in the previous sections, the scattering problem of a dielectric half-cylinder which is illuminated by a transmission wave can be obtained by the matrix equation [9]

$$[A][E] = [E^i] \tag{3.27}$$

where

$$E^i = e^{jk(x_m \cos\phi_i + y_m \sin\phi_i)} \tag{3.28}$$

and

$$\begin{aligned} A_{mn} &= \epsilon_m + j\frac{\pi}{2}(\epsilon_m - 1)ka_n H_1^{(2)}(ka_m) \qquad for \qquad m = n \\ &= j\frac{\pi}{2}(\epsilon_m - 1)ka_n J_1^{(2)}(ka_n) H_0^{(2)}(k\rho_{mn}) \qquad for \qquad m \neq n \end{aligned} \tag{3.29}$$

with

$$\rho_{mn} = \sqrt{(x_m - x_n)^2 + (y_m - y_n)^2} \tag{3.30}$$

for $m, n = 1, 2, ..., N$ by N as the number of cells the cylinder is divided into. ϵ_m is the average dielectric constant of cell m and a_m is the radius of the equivalent circular cell by the same cross section as cell m. E is the field inside the dielectric half-cylinder and $J_1^{(2)}$ is the Bessel function [11]; $H_1^{(2)}$ and $H_0^{(2)}$ are Hankel functions of the first and second kinds.

3.3.1 Green's Functions and Eigenfunctions

If the eigenvalue problem associated with the operator L can be solved, then one may find the associated Green's function. It is known that the eigenvalue problem

$$Lu = \lambda u, \quad a < x < b \tag{3.31}$$

by prescribed boundary conditions , has infinite many eigenvalues and corresponding orthonormal eigenfunctions as λ_n and ϕ_n, respectively, where $n = 1, 2, 3, ...$ Moreover, the eigenfunctions form a basis for the square integrable functions on the interval (a, b). Therefore it is assumed that the solution u is given in terms of eigenfunctions as

$$u(x) = \sum_{n=1}^{\infty} c_n \phi_n(x) \tag{3.32}$$

where the coefficients c_n are to be determined. Further, the given function f forms the source term in the nonhomogeneous differential equation

$$Lu = f \qquad or \qquad u = L^{-1} f$$

where L^{-1} is the opposite operator to the operator L. Now, the given function f can be written in terms of the eigenfunctions as

$$f(x) = \sum_{n=1}^{\infty} f_n \phi_n(x), \tag{3.33}$$

with

$$f_n = \int_a^b f(\xi)\phi_n(\xi)d\xi \tag{3.34}$$

Combining (3.32), (3.33), and (3.34) gives

$$L\left(\sum_{n=1}^{\infty} c_n \phi_n(x)\right) = \sum_{n=1}^{\infty} f_n \phi_n(x) \tag{3.35}$$

By the linear property associated with superposition principle , it can be shown that

$$L\left(\sum_{n=1}^{\infty} c_n \phi_n(x)\right) = \sum_{n=1}^{\infty} c_n L(\phi_n(x)) \tag{3.36}$$

But

$$\sum_{n=1}^{\infty} c_n L(\phi_n(x)) = \sum_{n=1}^{\infty} c_n \lambda_n \phi_n(x) = \sum_{n=1}^{\infty} f_n \phi_n(x) \tag{3.37}$$

which finally yields

$$L\left(\sum_{n=1}^{\infty} c_n \phi_n(x)\right) = \sum_{n=1}^{\infty} f_n \phi_n(x) \tag{3.38}$$

By comparing the above equations, it will be obtained that

$$c_n = \frac{1}{\lambda_n} \text{ and } f_n = \frac{1}{\lambda_n}\int_a^b f(\xi)\phi_n(\xi)d\xi \text{ for } n = 1, 2, 3, ... \tag{3.39}$$

Further

$$\begin{aligned} u(x) &= \sum_{n=1}^{\infty} c_n \phi_n(x) \qquad (3.40)\\ &= \sum_{n=1}^{\infty} \frac{1}{\lambda_n}\left(\int_a^b f(\xi)\phi_n(\xi)d\xi\right)\phi_n(x) \end{aligned}$$

Now, it is supposed that an interchange of summation and integral is allowed. In this case (3.40) can be written as

$$u(x) = \int_a^b \left(\sum_{n=1}^{\infty} \frac{\phi_n(x)\phi_n(\xi)}{\lambda_n}\right) f(\xi)d\xi \tag{3.41}$$

But by definition of Green's function, one may write

$$u(x) = L^{-1}f = \int_a^b g(x,\xi)f(\xi)d\xi \tag{3.42}$$

By comparing the last two equations, $u(x)$ can be expressed in terms of Green's functions as

$$g(x,\xi) = \sum_{n=1}^{\infty} \frac{\phi_n(x)\phi_n(\xi)}{\lambda_n} \tag{3.43}$$

is the Green's function associated with the eigenvalue problem (3.31) with the differential operator L.

3.4 The Method of Images

Solution of electromagnetic fields is greatly supported and facilitated by mathematical theorems in vector analysis. Maxwell's equations are based on Helmholtz's theorem where it is verified that a vector is uniquely specified by giving its divergence and curl, within a simply connected region and its normal component over the boundary. This can be proved as a mathematical theorem in a general manner [11]. Solving partial differential equations (PDE) like Maxwell's equation desires different methods, depending on, for instance, which boundary condition the PDE has and in which physical field it is studied.

The Green's function modeling is an applicable method to solve Maxwell's equations for some frequently used cases by different boundary conditions. The issue in this type of formulation is, in the first hand, determining and solving the appropriate Green's function by its boundary condition. Once the Green's function is determined, one may receive a clue to the physical interpretation of the whole problem and hence a better understanding of it. This forms the general manner of applying Green's function formulation in different fields of science. In some cases within electromagnetic modeling, where the physical source is in the vicinity of a perfectly electric conducting (PEC) surface and where there is some kind of symmetry in the geometry of the problem, the method of images will be a logical and facilitating method to determine the appropriate Green's function. The method of images is, in its turn, based on the uniqueness theorem verifying that a solution of an electrostatic problem satisfying the boundary condition is the only possible solution [12]. Electric- and magnetic- field of an infinitesimal dipole in the vicinity of an infinite PEC surface is one of the subjects that can be studied and facilitated by applying the method of images.

In the following section, the method of images is applied to derive the electromagnetic modeling for different electrical sources above a PEC surface.

3.4.1 The Electric Field for Sources above a PEC Surface

It is assumed that an electric point charge q is located at a vertical distance $y = r$ above an appropriate large conducting plane which is grounded. It will be difficult to apply

the ordinary field solution in this case but by image methods where an equivalent system is presented, it will be considerably easier to solve the original problem. An equivalent problem can be to place an image point charge $-q$ at the opposite side of the PEC plane, i.e. $y = -r$. In the equivalent problem, the boundary condition is not changed and a solution to the equivalent problem will be the only correct solution. The potential at the arbitrary point $P(x, y, z)$ is [13]

$$\Phi(x, y, z) = \frac{q}{4\pi\epsilon_0}\left(\frac{1}{\sqrt{x^2 + (y-r)^2 + z^2}} - \frac{1}{\sqrt{x^2 + (y+r)^2 + z^2}}\right) \tag{3.44}$$

which is a contribution from both charges q and $-q$ as

$$\Phi_+(x, y, z) = \frac{q}{4\pi\epsilon_0}\left(\frac{1}{\sqrt{x^2 + (y-r)^2 + z^2}}\right) \tag{3.45}$$

and

$$\Phi_-(x, y, z) = \frac{-q}{4\pi\epsilon_0}\left(\frac{1}{\sqrt{x^2 + (y+r)^2 + z^2}}\right) \tag{3.46}$$

respectively. According to the image methods, Eq. (3.44) gives the potential due to an electric point source above a PEC plane at the region $y > 0$. The field located at $y < 0$ will be zero; it is indeed the region where the image charge $-q$ is located.

Now it is assumed that a long line charge of constant charge λ per unit length is located at a distance d from a surface of a grounded conductor, occupying half of the all space. It is also assumed that the line charge is parallel to both the grounded plane and to the z-axis in the rectangular coordinate system. Further, the surface of the conducting grounded plane is coincided with yz-plane and x-axis passes through the line charge so that the boundary condition for this system is $\Phi(0, y, z) = 0$ where Φ is defined as the electric potential. To find the potential everywhere for this system by applying the method of images, one may start by converting this system to an equivalent system where the boundary condition of the original problem will be preserved. To solve this problem by method of images, the original system will first be converted to an another system where the conducting grounded plane is vanished, i.e. a system where the line charge is in free-space. By using the polar coordinate system, the potential at an arbitrary point P, see Fig. 3.1, is

$$\Phi(R, \phi) = \frac{\lambda}{2\pi\epsilon_0} \ln\left[\frac{(4L_2L_1)^{1/2}}{R}\right] \tag{3.47}$$

An equivalent problem may consist of a system of two parallel long lines with opposite charges in free-space and by a distance of $2d$ from each other; the charge densities of the two lines are assumed to be λ and $-\lambda$ respectively. According to the method of images, the total potential Φ will be determined by contribution from these two line charges which respectively are

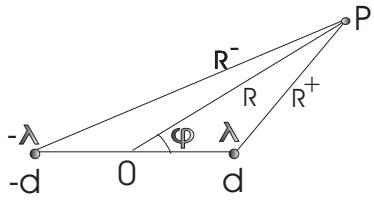

(a)

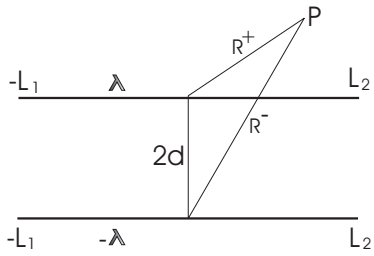

(b)

Figure 3.1: Geometry of two opposite long line charges, λ and $-\lambda$ by a distance of $2d$ from each other and observed as (a): perpendicular to the paper plane, (b): coincided by the paper plane.

$$\Phi^+ = \frac{\lambda}{2\pi\epsilon_0} \ln\left[\frac{(4L_2L_1)^{1/2}}{R^+}\right] \tag{3.48}$$

and

$$\Phi^- = -\frac{\lambda}{2\pi\epsilon_0} \ln\left[\frac{(4L_2L_1)^{1/2}}{R^-}\right] \tag{3.49}$$

The total potential is resulted from both of these two line charges as

$$\begin{aligned} \Phi &= \Phi^+ + \Phi^- \\ &= \frac{\lambda}{2\pi\epsilon_0} \ln\left(\frac{R^-}{R^+}\right) \\ &= \frac{\lambda}{2\pi\epsilon_0} \ln\left(\frac{d^2 + R^2 + 2dR\cos\phi}{d^2 + R^2 - 2dR\cos\phi}\right) \end{aligned} \tag{3.50}$$

According to uniqueness theorem and the method of images, Eq. (3.50) gives the solution for a long line charge by a distance of d above a PEC plane. The potential below the PEC surface will be zero. This is illustrated in Fig. 3.2

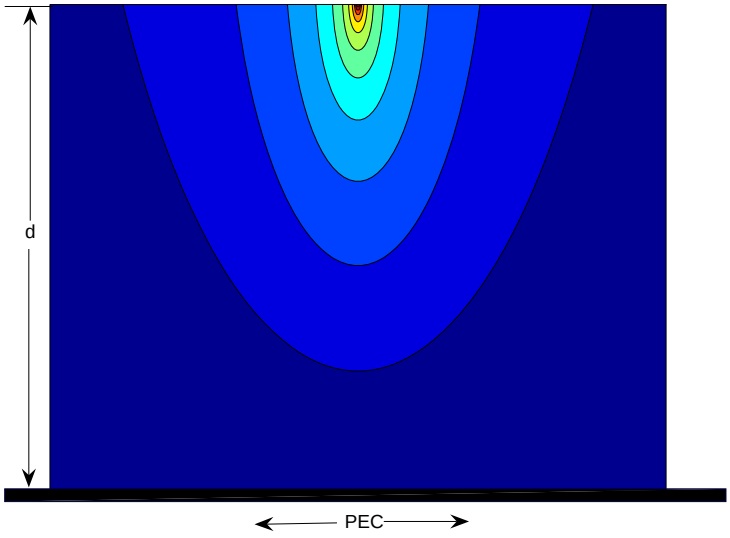

Figure 3.2: Electric potential of an infinitely long line charge parallel to a PEC surface and by a height of d above it.

3.4.2 Radiated Electric Field of an Infinitesimal Dipole above a PEC Surface

The overall radiation properties of a radiating system can significantly alter in the vicinity of an obstacle. The ground as a lossy medium, i.e. $\sigma \neq 0$, is expected to act as a very good conductor above a certain frequency. Hence, by applying the method of images the ground should be assumed as a perfect electric conductor, flat, and infinite in extent for facilitating the analysis. It will also be assumed that any energy from the radiating element towards the ground undergoes reflection and the ultimate energy amount is a summation of the reflective and directed (incident) components where the reflected component can be accounted for by the the introduction of the image sources. In all of the following cases, the far-field observation is considered. To find the electric field, radiated by a current element along the infinitesimal length l', it will be convenient to use the magnetic vector potential $\mathbf{A}$ as [14]

$$\mathbf{A}(x,y,z) = \frac{\mu}{4\pi}\int_C \mathbf{I}(x',y',z')\frac{e^{-j\beta R}}{R}dl' \tag{3.51}$$

where (x,y,z) and (x',y',z') represent the observation point coordinates and the coordinate for the constant electric current source $\mathbf{I}$, respectively. R is the distance from any point on the source to the observation point; the integral path C is the length of the

source and $\beta^2 = \omega^2\mu\epsilon$ where μ and ϵ are permeability and permittivity of the medium. By the assumption that an infinitesimal dipole is placed along the z-axis of a rectangular coordinate system plus that it is placed on the origin, one may write $\mathbf{I} = \hat{z}I_0$ for constant electric current I_0, and $x' = y' = z' = 0$. Hence, the distance R will be

$$R = \sqrt{(x-x')^2 + (y-y')^2 + (z-z')^2} = \sqrt{x^2+y^2+z^2} \tag{3.52}$$

By knowing that $dl' = dz'$, and by setting $r = \sqrt{x^2+y^2+z^2}$, Eq. (3.51) may be written as

$$\mathbf{A}(x,y,z) = \hat{z}\frac{\mu I_0}{4\pi r}e^{-j\beta r}\int_{-l/2}^{l/2} dz' = \hat{z}\frac{\mu I_0 l}{4\pi r}e^{-j\beta r} \tag{3.53}$$

The most appropriate coordinate system for studying such cases is the spherical coordinate system why the vector potential in Eq. (3.53) should be converted into the spherical components as

$$A_r = A_z\cos\theta = \frac{\mu I_0 l}{4\pi r}e^{-j\beta r}\cos\theta \tag{3.54}$$

$$A_\phi = -A_z\sin\theta = -\frac{\mu I_0 l}{4\pi r}e^{-j\beta r}\sin\theta \tag{3.55}$$

$$A_\phi = 0 \tag{3.56}$$

In the last three equations, $A_x = A_y = 0$ by the assumption that the infinitesimal dipole is placed along the z-axis. For determining the electric field radiation of the dipole, one should operate the magnetic vector potential $\mathbf{A}$ by a curl operation to obtain the magnetic field intensity $\mathbf{H}_A$ as

$$\mathbf{H}_A = \frac{1}{\mu}\nabla\times\mathbf{A} \tag{3.57}$$

In spherical coordinate system, Eq. (3.57) is expressed as

$$\mathbf{H}_A = \frac{1}{\mu}\left(\hat{r}\frac{1}{r\sin\theta}\left[\frac{\partial}{\partial\theta}(A_\phi\sin\theta) - \frac{\partial A_\theta}{\partial A_\phi}\right] + \frac{\hat{\theta}}{r}\left[\frac{1}{\sin\theta}\frac{\partial A_r}{\partial\phi} - \frac{\partial}{\partial r}(rA_\phi)\right] + \frac{\hat{\phi}}{r}\left[\frac{\partial}{\partial r}(rA_\theta) - \frac{\partial A_r}{\partial\theta}\right]\right)$$

But according to Eq. (3.56) and due to spherical symmetry of the problem, where there are no ϕ-variations along z-axis, the last equation simplifies to [14]

$$\mathbf{H}_A = \frac{1}{\mu}\frac{\hat{\phi}}{r}\left[\frac{\partial}{\partial r}(rA_\theta) - \frac{\partial A_r}{\partial\theta}\right] \tag{3.58}$$

which together with (3.54) and (3.55) gives

$$\mathbf{H}_A = \hat{\phi}\frac{\beta I_0 l\sin\theta}{4\pi r}\left(1 + \frac{1}{j\beta r}\right)e^{-j\beta r} \tag{3.59}$$

Further, by equating Maxwell's equations, it will be obtained that

$$\nabla \times \mathbf{H}_A = \mathbf{J} + j\omega\epsilon\mathbf{E}_A \tag{3.60}$$

By setting $\mathbf{J} = 0$ in Eq. (3.60), it will be obtained that

$$\mathbf{E}_A = \frac{1}{j\omega\epsilon}\nabla \times \mathbf{H}_A \tag{3.61}$$

Eq. (3.61), together with Eqs. (3.54)-(3.56) yields

$$E_r = \eta\frac{I_0 l\cos\theta}{2\pi r^2}\left[1 + \frac{1}{j\beta r}\right]e^{-j\beta r} \tag{3.62}$$

$$E_\theta = j\eta\frac{\beta I_0 l\sin\theta}{4\pi r}\left[1 + \frac{1}{j\beta r} - \frac{1}{\beta r^2}\right]e^{-j\beta r} \tag{3.63}$$

$$E_\phi = 0 \tag{3.64}$$

where $\eta = E_\theta/H_\phi$ is called the intrinsic impedance ($= 377 \simeq 120\pi$ ohms for free-space). Stipulating for far-field region, i.e. a region where $\beta r >> 1$, the electric fields E_θ and E_r in Eqs. (3.62)-(3.64) can be approximated by

$$E_\theta \simeq j\eta\frac{\beta I_0 l\sin\theta}{4\pi r}\sin\theta \tag{3.65}$$

$$E_r \simeq E_\phi = 0 \tag{3.66}$$

which is the electric far-field solution for an infinitesimal dipole along z-axis and in the spherical coordinate system. The same procedure may be used to solve the electric field for an infinitesimal dipole along x-axis where the magnetic vector potential $\mathbf{A}$ is defined as

$$\mathbf{A} = \hat{\mathbf{x}}\frac{\mu I_0 l e^{-j\beta r}}{4\pi r} \tag{3.67}$$

In the spherical coordinate system, the above equation is expressed as

$$A_r = A_x\sin\theta\cos\phi \tag{3.68}$$

$$A_\theta = A_x\cos\theta\cos\phi \tag{3.69}$$

$$A_\phi = -A_x\sin\phi \tag{3.70}$$

It should be mentioned that $A_y = A_z = 0$ due to the placement of the infinitesimal dipole along x-axis. By far-field approximation, and based on Eqs. (3.68)-(3.70), the electric field can be written as

$$E_r \simeq 0 \tag{3.71}$$

$$E_\theta \simeq -j\omega A_\theta = -j\omega \frac{\mu I_0 l e^{-j\beta r}}{4\pi r} \cos\theta \cos\phi \tag{3.72}$$

$$E_\phi \simeq -j\omega A_\phi = -j\omega \frac{\mu I_0 l e^{-j\beta r}}{4\pi r} \sin\phi \tag{3.73}$$

The electric field, as a whole, will be contributions from both A_θ and A_ϕ which is expressed as

$$E_A \simeq -j\omega \left(A_\theta + A_\phi\right) = -j\omega \frac{\mu I_0 l e^{-j\beta r}}{4\pi r} \left(\cos\theta \cos\phi - \sin\phi\right) \tag{3.74}$$

3.4.3 Infinitesimal Vertical Dipole above a PEC Surface

The overall radiation properties of a radiating system can significantly alter in the vicinity of an obstacle. The ground as a medium is expected to act as a very good conductor above a certain frequency. Applying the method of images and for simplifying the analysis, the ground is assumed to be a perfect electric conductor, flat, and infinite in extent. It is also assumed that energy from the radiating element undergoes reflection and the ultimate energy amount is a summation of the reflective and the directed components respectively where the reflected component can be accounted for by the image sources.

A vertical dipole of infinitesimal length l and constant current I_0, is now assumed to be placed along z-axis by a distance d above a PEC surface by an infinite extent. The far-zone directed- and reflected- components in a far-field point P are respectively given by [15]

$$E_\theta^D \simeq j\eta \frac{\beta I_0 l e^{-j\beta r_1}}{4\pi r_1} \sin\theta_1 \tag{3.75}$$

and

$$E_\theta^R \simeq j\eta \frac{\beta I_0 l e^{-j\beta r_2}}{4\pi r_2} \sin\theta_2 \tag{3.76}$$

where r_1 and r_2 are the distances between the observation point and the two other points, the source- and the image- locations; θ_1 and θ_2 are the related angles between these lines and z-axis. It is intended to express all the quantities only by the elevation plane angle θ and the radial distance r between the observation point and the origin of the spherical

coordinate system. For this purpose, one may utilize the law of cosines an also a pair of simplifications regarding the far-field approximation. The law of cosines gives

$$r_1 = \sqrt{r^2 + d^2 - 2rd\cos\theta} \tag{3.77}$$

$$r_2 = \sqrt{r^2 + d^2 - 2rd\cos(\pi - \theta)} \tag{3.78}$$

By binomial expansion and regarding phase variations, one may write

$$r_1 = r - d\cos\theta \tag{3.79}$$

$$r_2 = r + d\cos\theta \tag{3.80}$$

By utilizing the far-zone approximation where $r_1 \simeq r_2 \simeq r$, and all of the above simplifications, it is obtained that

$$E_\theta^{total} = E_\theta^D + E_\theta^R = j\eta\frac{\beta I_0 l e^{-j\beta r}}{4\pi r}\sin\theta\left(e^{+j\beta d\cos\theta} + e^{-j\beta d\cos\theta}\right) \tag{3.81}$$

Finally, after some algebraic manipulations, one may find for $z \geq 0$

$$E_\theta^{total} = j\eta\frac{\beta I_0 l e^{-j\beta r}}{4\pi r}\sin\theta\left[2\cos(\beta d\cos\theta)\right] \tag{3.82}$$

According to the image theory, the field will be zero for $z < 0$.

Chapter 4

The PEEC Method and Application of Numerical Methods

This chapter describes the time domain PEEC formulation for orthogonal structures. Some basic concepts within electromagnetism are also introduced. It is also shown that how the PEEC method has been combined with the method of complex image methods (CIM). The parallel algorithm of Grid-PEEC for calculation of partial coefficients and frequency domain systems is also presented in this chapter.

4.1 Derivation of the PEEC Method

This presented derivation of the PEEC method is based, to a large extent, on the work presented in [16].

4.1.1 Derivation of Electric Field Integral Equation

The theoretical derivation of the PEEC method starts from the expression of the total electric field in free space, $\vec{E}^T(\vec{r},t)$, by using the magnetic vector and electric scalar potentials, $\vec{A}$ and ϕ respectively.

$$\vec{E}^T(\vec{r},t) = \vec{E}^i(\vec{r},t) - \frac{\partial \vec{A}(\vec{r},t)}{\partial t} - \nabla\phi(\vec{r},t) \tag{4.1}$$

where $\vec{E}^i$ is a potential applied external electric field. If the observation point, $\vec{r}$, is on the surface of a conductor, the total electric field can be written as

$$\vec{E}^T(\vec{r},t) = \frac{\vec{J}(\vec{r},t)}{\sigma} \tag{4.2}$$

in which $\vec{J}(\vec{r},t)$ is the current density in a conductor and σ is the conductivity of the conductor. Combining the above equations results in

$$\vec{E}^i = \frac{\vec{J}(\vec{r},t)}{\sigma} + \frac{\partial \vec{A}(\vec{r},t)}{\partial t} + \nabla\phi(\vec{r},t) \tag{4.3}$$

To transform (4.3) into the electric field integral equation (EFIE) the definitions of the electromagnetic potentials, $\vec{A}$ and ϕ are used. The magnetic vector potential, $\vec{A}$, at the observation point $\vec{r}$ is given by

$$\vec{A}(\vec{r},t) = \sum_{k=1}^{K} \mu \int_{v_k} G(\vec{r},\vec{r}\prime)\vec{J}(\vec{r}\prime,t_d)dv_k \tag{4.4}$$

in which the summation is over K conductors and μ is the permeability of the medium. Since no magnetic material medium are considered in this thesis $\mu = \mu_0$. In (4.4) the free space Green's function is used and is defined as

$$G(\vec{r},\vec{r}\prime) = \frac{1}{4\pi}\frac{1}{|\vec{r}-\vec{r}\prime|} \tag{4.5}$$

$\vec{J}$ is the current density at a source point $\vec{r}\prime$ and t_d is the retardation time between the observation point, $\vec{r}$, and the source point given by

$$t_d = t - \frac{|\,\vec{r}-\vec{r}\prime\,|}{c} \tag{4.6}$$

where $c = 3 \cdot 10^8 m/s$. The electric scalar potential, ϕ, at the observation point $\vec{r}$ is given by

$$\phi(\vec{r}, t) = \sum_{k=1}^{K} \frac{1}{\epsilon_0} \int_{v_k} G(\vec{r}, \vec{r\prime}) q(\vec{r\prime}, t_d) dv_k \tag{4.7}$$

in which ϵ_0 is the permittivity of free space and q is the charge density at the source point. Combining (4.3), (4.4) and (4.7) results in the well known *electric field integral equation* (EFIE) or *mixed potential integral equation* (MPIE) that is to be solved according to

$$\begin{aligned} \hat{n} \times \vec{E}^i(\vec{r}, t) &= \hat{n} \times \left[\frac{\vec{J}(\vec{r}, t)}{\sigma} \right] \\ &+ \hat{n} \times \left[\sum_{k=1}^{K} \mu \int_{v_k} G(\vec{r}, \vec{r\prime}) \frac{\partial \vec{J}(\vec{r\prime}, t_d)}{\partial t} \, dv_k \right] \\ &+ \hat{n} \times \left[\sum_{k=1}^{K} \frac{\nabla}{\epsilon_0} \int_{v_k} G(\vec{r}, \vec{r\prime}) q(\vec{r\prime}, t_d) \, dv_k \right] \end{aligned} \tag{4.8}$$

where $\hat{n}$ is the surface normal to the body surfaces. The transformation of the EFIE in (4.8) into the PEEC formulation starts by expanding the current- and charge-densities according to this section. This results in a general form of the EFIE for the PEEC formulation from which the equivalent circuit can be derived.

4.1.2 PEEC Current Density Expansion

The total current density, $\vec{J}$, in (4.8) is expanded in the PEEC formulation to include the conduction current density, $\vec{J}^C$, due to the losses in the material and a polarization current density, $\vec{J}^P$, due to the dielectric material properties resulting in

$$\vec{J} = \vec{J}^C + \vec{J}^P \tag{4.9}$$

where

$$\vec{J}^C = \sigma \vec{E} \tag{4.10}$$

$$\vec{J}^P = \epsilon_0(\epsilon_r - 1)\frac{\partial \vec{E}}{\partial t} \tag{4.11}$$

For perfect conductors, the total current density $\vec{J}$ reduces to $\vec{J}^C$. While for perfect dielectrics the total current density reduces to $\vec{J}^P$. The polarization current density is added in the differential form of the generalized Ampere's circuital law according to

$$\nabla \times \vec{H} = \vec{J}^C + \epsilon_0(\epsilon_r - 1)\frac{\partial \vec{E}}{\partial t} + \epsilon_0 \frac{\partial \vec{E}}{\partial t} \tag{4.12}$$

which is reduced to the original form

$$\nabla \times \vec{H} = \vec{J}^C + \epsilon_0 \frac{\partial \vec{E}}{\partial t} \tag{4.13}$$

for $\epsilon_r = 1$. In this way the displacement current due to the bound charges for the dielectrics with $\epsilon_r > 1$ are treated separately from the conduction currents due to the free charges.

4.1.3 PEEC Charge Density Expansion

The charge density q^T, indicating the combination of the free, q^F, and bound, q^B, charge density is given by

$$q^T = q^F + q^B \tag{4.14}$$

This allows the modeling of the displacement current due to the bound charges for dielectrics with $\epsilon_r > 1$ separately from the conducting currents due to the free charges. For perfect conductors, the total charge density q^T reduces to q^F. While for perfect dielectrics the total charge density reduces to q^B. The resulting EFIE for the PEEC formulation can then be written as

$$\begin{aligned}
\hat{n} \times \vec{E}^i(\vec{r},t) &= \hat{n} \times \left[\frac{\vec{J}^C(\vec{r},t)}{\sigma} \right] \\
&+ \hat{n} \times \left[\sum_{k=1}^{K} \mu \int_{v_k} G(\vec{r},\vec{r}\prime) \frac{\partial \vec{J}^C(\vec{r}\prime,t_d)}{\partial t} \, dv_k \right] \\
&+ \hat{n} \times \left[\sum_{k=1}^{K} \epsilon_0(\epsilon_r - 1)\mu \int_{v_k} G(\vec{r},\vec{r}\prime) \frac{\partial^2 \vec{E}(\vec{r}\prime,t_d)}{\partial t^2} \, dv_k \right] \\
&+ \hat{n} \times \left[\sum_{k=1}^{K} \frac{\nabla}{\epsilon_0} \int_{v_k} G(\vec{r},\vec{r}\prime) q^T(\vec{r}\prime,t_d) \, dv_k \right]
\end{aligned} \tag{4.15}$$

4.1.4 Interpretation as Equivalent Circuit

The conversion from integral equation, (4.15), to equivalent circuit formulation is detailed in this section. The PEEC formulation for a strict conductor environment is detailed, for the dielectric formulation review reference [17]. The exclusion of dielectric bodies and external fields reduces (4.15) to

$$\begin{aligned}
0 &= \hat{n} \times \left[\frac{\vec{J}^C(\vec{r},t)}{\sigma} \right] \\
&+ \hat{n} \times \left[\sum_{k=1}^{K} \mu \int_{v_k} G(\vec{r},\vec{r}\prime) \frac{\partial \vec{J}^C(\vec{r}\prime,t_d)}{\partial t} \, dv_k \right] \\
&+ \hat{n} \times \left[\sum_{k=1}^{K} \frac{\nabla}{\epsilon_0} \int_{v_k} G(\vec{r},\vec{r}\prime) q^F(\vec{r}\prime,t_d) \, dv_k \right]
\end{aligned} \tag{4.16}$$

Note that the system of equations in (4.16) have two unknowns, the conduction current density, $\vec{J}^C$, and the charge density, q^F. To solve the system of equations the following procedure is employed :

1. *The current densities* are discretized into volume cells that gives a 3D representation of the current flow. This is done by defining rectangular pulse functions

$$P_{\gamma nk} = 1, inside\ \ the\ \ nk:th\ \ volume\ \ cell \qquad (4.17)$$
$$0, \ \ elsewhere$$

where $\gamma = x, y, z$ indicates the current component of the n:th volume cell in the k:th conductor.

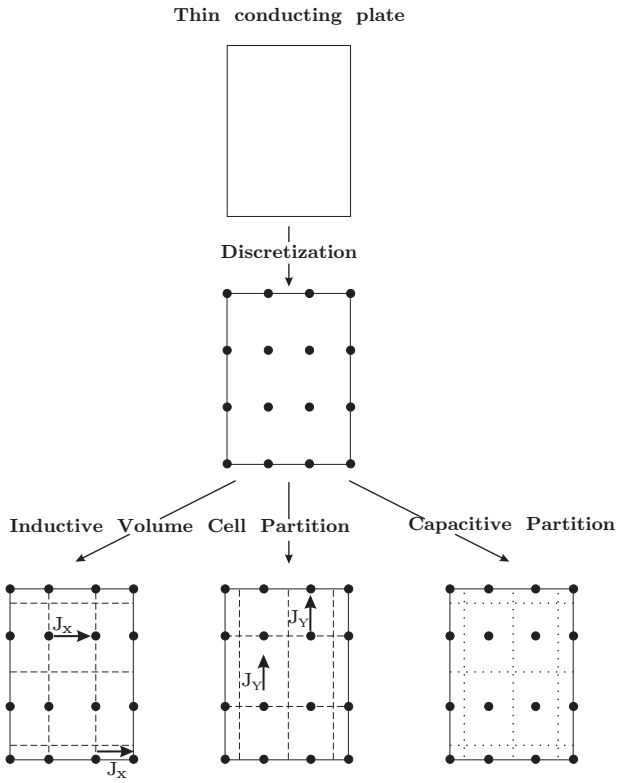

Figure 4.1: 2-D Discretization of current density and surface charge distribution.

2. *The charge densities* are discretized into surface cells that gives a 2D representation of the charge over the corresponding volume cell, Fig. 4.1 This is done by defining

the rectangular pulse functions

$$p_{mk} = 1, inside\ \ the\ \ mk:th\ \ surface\ \ cell \qquad (4.18)$$
$$0, elsewhere$$

for the charge density on the m:th volume cell of the k:th conductor. Using the definitions in (4.17) and (4.18) the current and charge densities can be written as

$$\vec{J}^C_{\gamma k}(\vec{r}\prime, t_d) = \sum_{n=1}^{N_{\gamma k}} P_{\gamma nk}\ J_{\gamma nk}(\vec{r}_{\gamma nk}\prime, t_{\gamma nk}) \qquad (4.19)$$

$$q^T_k(\vec{r}\prime, t_d) = \sum_{m=1}^{M_k} p_{mk}\ q_{mk}(\vec{r}_{mk}\prime, t_{mk}) \qquad (4.20)$$

where

$$t_{\gamma nk} = t - \frac{|\vec{r} - \vec{r}_{\gamma nk}\prime|}{v} \qquad (4.21)$$
$$t_{mk} = t - \frac{|\vec{r} - \vec{r}_{mk}\prime|}{v}$$

The vector $\vec{r}_{\gamma nk}\prime$ is the source position vector indicating the center of the n:th volume cell of the k:th conductor in the γ discretization and $\vec{r}_{mk}\prime$ is the source position vector indicating the center of the m:th surface cell of the k:th conductor. In (4.19), the summation is over all the volume cells in conductor k with γ directed current while in (4.20), the summation is over all the surface cells in conductor k.

Pulse functions are also used for the testing functions resulting in a Galerkin solution. The inner product is defined as a weighted volume integral over a cell as

$$< f, g >= \frac{1}{a} \int_v f(\vec{r}) g(\vec{r})\ dv \qquad (4.22)$$

Combining (4.16), (4.19), (4.20), and (4.22) while using the inner product defined in (4.31) results in a systems of equations given by

$$\begin{aligned} 0 &= \hat{n} \times \left[\frac{\vec{J}^C(\vec{r}, t)}{\sigma} \right] \\ &+ \hat{n} \times \left[\sum_{k=1}^{K} \sum_{n=1}^{N\gamma k} \mu \int_{v\prime} \int_{v_{\gamma nk}} G(\vec{r}, \vec{r}_{\gamma nk}\prime) \frac{\partial P_{\gamma nk} J_{\gamma nk}(\vec{r}_{\gamma nk}\prime, t_{\gamma nk})}{\partial t}\ dv_{\gamma nk} dv\prime \right] \\ &+ \hat{n} \times \left[\sum_{k=1}^{K} \sum_{m=1}^{Mk} \frac{\nabla}{\epsilon_0} \int_{v_{mk}} G(\vec{r}, \vec{r}_{mk}\prime) p_{mk} q_{mk}(\vec{r}_{mk}\prime, t_{mk})\ dv_{mk} \right] \end{aligned} \qquad (4.23)$$

Equation 4.23 is the basic discretized version of the electric field integral equation for the PEEC method from which the partial elements can be identified as will be shown in the following paragraphs.

4.1.4.1 Partial Inductances

The basic expression for partial inductances can be derived from the second term in (4.23) by using :

- The free-space Green's function.
- The expression $I_{\gamma m} = J_{\gamma m} a_m$ for the total current, $I_{\gamma m}$, through a cross sectional area, a_m.

This results in

$$\sum_{k=1}^{K} \sum_{n=1}^{N\gamma k} \frac{\mu}{4\pi} \frac{1}{a_{v\prime}\, a_{v_{\gamma nk}}} \int_{v\prime} \int_{v_{\gamma nk}} \frac{\frac{\partial}{\partial t} I_{\gamma nk}(\vec{r}_{\gamma nk}\prime, t_{\gamma nk})}{|\vec{r} - \vec{r}\prime|}\, dv_{\gamma nk} dv\prime \tag{4.24}$$

and can be interpreted as the inductive voltage drop, v_L, over the corresponding volume cell. By defining the partial inductance as

$$Lp_{\alpha\beta} = \frac{\mu}{4\pi} \frac{1}{a_\alpha a_\beta} \int_{v_\alpha} \int_{v_\beta} \frac{1}{|\vec{r_\alpha} - \vec{r_\beta}|} dv_\alpha dv_\beta \tag{4.25}$$

can be rewritten as

$$v_L = \sum_{k=1}^{K} \sum_{n=1}^{N\gamma k} Lp_{v\prime\, \gamma nk} \frac{\partial}{\partial t} I_{\gamma nk}(t - \tau_{v\prime\, v_{\gamma nk}}) \tag{4.26}$$

where $\tau_{v\prime\, v_{\gamma nk}}$ is the center to center delay between the volume cells $v\prime$ and $v_{\gamma nk}$. Equation 4.25 is the basic definition for the partial self and mutual inductance using the volume formulation. It is from this definition that simplified and analytical formulas for the partial inductances for special geometries have been developed. The interpretation of the second term in (4.23) as the inductive voltage drop (using the partial inductance concept) results in :

- The connection of nearby nodes using the partial self inductance ($Lp_{\alpha\alpha}$) of the corresponding volume cell (α).
- The mutual inductive coupling of all volume cells using the concept of partial mutual inductance.

A voltage source has been used to sum all the inductive (magnetic field) couplings from all other volume cells, corresponding to the summation in (4.27). This voltage source is defined as

$$V_m^L(t) = \sum_{\forall n, n \neq m} L_{p_{mn}} \frac{\partial i_n(t - \tau_{mn})}{\partial t} \tag{4.27}$$

Where $i_n(t - \tau_{mn})$ is the current through volume cell n at an earlier instance in time, $(t - \tau_{mn})$. A PEEC model only consisting of partial inductances is entitled a (L_p)PEEC model.

4.1.4.2 Coefficients of Potential

The basic definition for partial coefficients of potential can be derived from the third term in (4.23) by using the following approximations :

- The charges only resides on the surface of the volumes, i.e. converting the volume integral to a surface integral.
- The integral in the γ coordinate can be calculated using a finite difference (FD) approximation according to

$$\int_v \frac{\partial}{\partial \gamma} F(\gamma) dv \approx a \left[F\left(\gamma + \frac{l_m}{2}\right) - F\left(\gamma - \frac{l_m}{2}\right) \right] \tag{4.28}$$

This results in

$$\sum_{k=1}^{K} \sum_{m=1}^{M_k} \left[q_{mk}(t_{mk}) \frac{1}{4\pi\epsilon_0} \int_{S_{mk}} \frac{1}{|\vec{r}^{+} - \vec{r\prime}|} ds\prime - q_{mk}(t_{mk}) \frac{1}{4\pi\epsilon_0} \int_{S_{mk}} \frac{1}{|\vec{r}^{-} - \vec{r\prime}|} ds\prime \right] \tag{4.29}$$

which can be interpreted as the capacitive voltage drop, v_C, over the actual cell and the vectors $\vec{r}^{+}$ and $\vec{r}^{-}$ are associated with the positive and negative end of the cell respectively. By defining the partial coefficient of potential as

$$p_{ij} = \frac{1}{S_i S_j} \frac{1}{4\pi\epsilon_0} \int_{S_i} \int_{S_j} \frac{1}{|\vec{r_i} - \vec{r_j}|} \, dS_j \, dS_i \tag{4.30}$$

the capacitive voltage drop can be written as

$$v_C = \sum_{k=1}^{K} \sum_{m=1}^{M_k} Q_{mk}(t - t_{mk}) [pp^{+}_{i(mk)} - pp^{-}_{i(mk)}] \tag{4.31}$$

using the total charge, Q_{mk}, of the mk:th cell.
From the basic definition in (4.30) a number of simplified and analytical formulas for partial coefficients of potential can be derived for special geometries configurations. The interpretation of the third term in (4.23) as self and mutual (partial) coefficient of potential (capacitive) coupling results in :

- The connection of each surface cell (node) to infinity through self partial (*pseudo-*) capacitances.
- Mutual capacitive couplings of all surface cells (nodes).

The voltage source, V_i^C which has been used to sum all the capacitive (electric field) couplings from all other surface cells, is defined as

$$V_i^C(t) = \sum_{\forall j, j \neq i} \frac{P_{ij}}{P_{jj}} V_{C_j}(t - \tau_{ij}) \tag{4.32}$$

where $V_{C_j}(t - \tau_{ij})$ is the voltage over the pseudo-capacitance, $\frac{1}{P_{jj}}$, of the j:th node, at an earlier instance in time, $(t - \tau_{ij})$. A PEEC model only consisting of partial coefficients of potential is entitled a (P)PEEC model.

4.1.4.3 Resistances

The first term in (4.23) can be shown to equal the resistive voltage drop over the volume cell. By assuming a constant current density over the volume cell the term is rewritten as

$$\frac{\vec{J}_\gamma^C}{\sigma_\gamma} = \frac{I_\gamma}{a_\gamma \sigma_\gamma} \tag{4.33}$$

where a_γ is the cross section of the volume cell normal to the γ direction. The resistance is then calculated as

$$R_\gamma = \frac{l_\gamma}{a_\gamma \sigma_\gamma} \tag{4.34}$$

where l_γ is the volume cell length in the γ direction.The interpretation of the first term in (4.23) as the voltage drop in a conductor results in a lumped resistance connection between the nodes in the PEEC model. A PEEC model only consisting of volume cell resistances is entitled a (R)PEEC model.

4.1.4.4 Combined (L_p)PEEC, (P)PEEC, and (R)PEEC Models.

When partial inductances are used in the (R)PEEC model a series connection of the resistance and partial inductance is made. This results in a (L_p, R)PEEC model. The inclusion of partial coefficients of potential results in a (L_p, R, P)PEEC model, Fig. 4.2. In the figure, one surface cell at each node is used to account for the capacitive coupling to corresponding node.

4.1.5 Solution of Time- and Frequency Domain PEEC Models

For the solution of PEECs in the time and frequency domain an *Admittance Method* or a *Modified Nodal Analysis* (MNA) [18] method can be used. The Admittance Method produces a minimal but dense system matrix to obtain the voltages in the structure. The MNA solves for both voltages and currents in a structure and therefore produces a larger, and sparse, system matrix. The MNA method is widely used in modern circuit analysis software due to its full-spectrum properties and flexibility to include additional circuit elements. The choice between the two methods depends on the specific problem at hand and the computational resources available.

4.2 Practical PEEC Modeling

The basic procedure for creating PEEC models is illustrated in Fig. 4.3 illustrating all the essential blocks required in a PEEC based electromagnetic solver. Shortly, a graphical tool is needed to draw and edit a structure, a routine then performs the discretization of the structure, the PEEC engine then calculates the partial elements and creates and solves the linear system (for both time and frequency domain simulations). Finally, if the system is stable, the solution variables (currents and voltages) are exported to a graph viewer for further inspection.

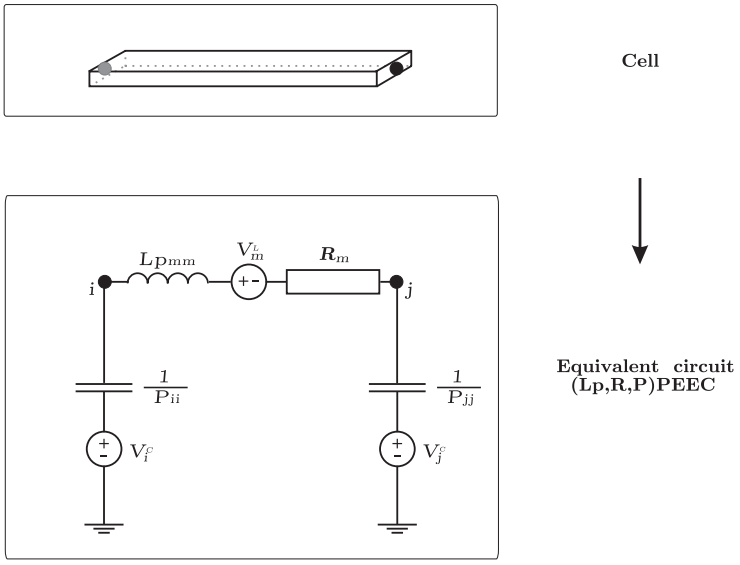

Figure 4.2: (L_p, R, P)PEEC model for volume cell m connecting node i and j.

4.3 The Parallel Algorithm of Grid-PEEC

By defining a grid as a system of distributed computers via a network, the main purpose of Grid PEEC computing is to improve the computational time by an object-oriented code which is more time efficient, more structured, and less memory consuming. Grid (parallel) computing is of practical importance where there is no availability to super computers for solving numerically large problems. A major issue within parallel computing is that if/how the main problem can be divided into sub-problems which will be solved by several processing units. The communication time between these processing units is an another crucial issue.

In the nonorthogonal PEEC method, conductors and dielectrics, can be both orthogonal and non-orthogonal quadrilateral (surface) and hexahedral (volume) elements. The formulation utilizes a global and a local coordinate system where the global coordinate system uses orthogonal coordinates x, y, z where a global vector $\vec{F}$ is defined as $\vec{F} = F_x\vec{x} + F_y\vec{y} + F_z\vec{z}$. A vector in the global coordinates are marked as $\vec{r_g}$. The local coordinates a, b, c are used to separately represent each specific possibly non-orthogonal object and the unit vectors are $\vec{a}$, $\vec{b}$, and $\vec{c}$, see further [19] and Fig. 4.4. The model in Fig. 4.5 consists of:

- partial inductances (L_p) which are calculated from the volume cell discretization using a double volume integral.
- coefficients of potentials which are calculated from the surface cell discretization

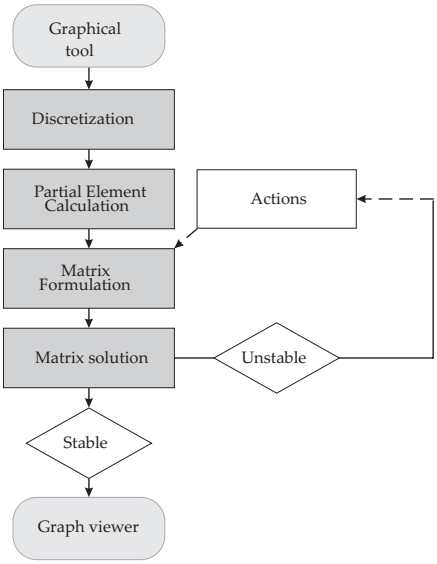

Figure 4.3: Work flow when creating PEEC models.

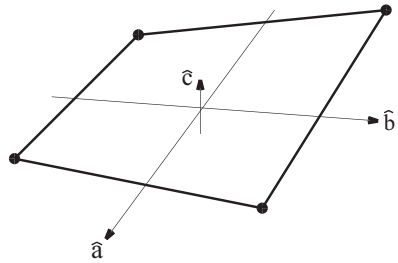

Figure 4.4: Nonorthogonal element created by the mesh generator with associated local coordinate system.

using a double surface integral.

- retarded current controlled current sources, to account for the electric field couplings, given by $I_p^i = \frac{p_{ij}}{p_{ii}} I_C^j(t - t_{d_{ij}})$ where $t_{d_{ij}}$ is the free space travel time (delay time) between surface cells i and j,

- retarded current controlled voltage sources, to account for the magnetic field couplings, given by $V_L^n = Lp_{nm} \frac{\partial I_m(t-t_{d_{nm}})}{\partial t}$, where $t_{d_{nm}}$ is the free space travel time (delay time) between volume cells n and m.

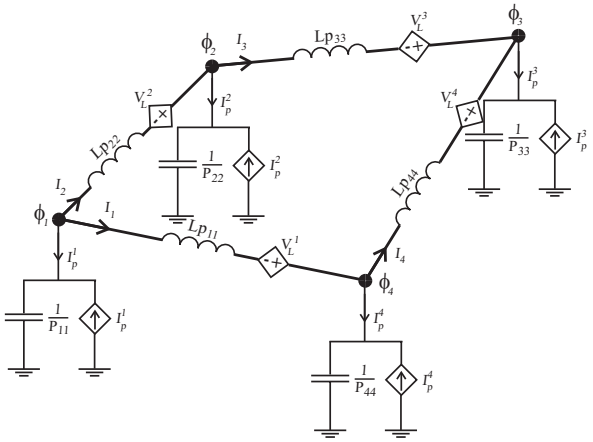

Figure 4.5: (L_p,P,τ)PEEC model for metal patch in Fig. 4.4 discretized with four edge nodes. Controlled current sources, I_p^n, account for the electric field coupling and controlled voltage sources, V_L^n, account for the magnetic field coupling.

By using the MNA method, the PEEC model circuit elements can be placed in the MNA system matrix during evaluation by the use of correct matrix stamps [18]. The MNA system, when used to solve frequency domain PEEC models, can be schematically described as

$$\begin{array}{rcl} j\omega \boldsymbol{P}^{-1} V - \boldsymbol{A}^T I & = & I_s \\ \boldsymbol{A} V - (\boldsymbol{R} + j\omega \boldsymbol{L}_p) I & = & V_s \end{array} \tag{4.35}$$

where: $\boldsymbol{P}$ is the coefficient of potential matrix, $\boldsymbol{A}$ is a sparse matrix containing the connectivity information, $\boldsymbol{L}_p$ is a dense matrix containing the partial inductances, elements of the type Lp_{ij}, $\boldsymbol{R}$ is a matrix containing the volume cell resistances, V is a vector containing the node potentials (solution), elements of the type ϕ_i, I is a vector containing the branch currents (solution), elements of the type I_i, I_s is a vector containing the current source excitation, and V_s is a vector containing the voltage source excitation. The first row in the equation system in (4.35) is Kirchoff's current law for each node while the second row satisfy Kirchoff's voltage law for each basic PEEC cell (loop). The use of the MNA method when solving PEEC models is the preferred approach since additional active and passive circuit elements can be added by the use of the corresponding MNA stamp. For a complete derivation of the quasi-static and full-wave PEEC circuit equations using the MNA method, see for example [21].

4.3.1 Grid-PEEC by Alchemi

There exist various software for creating grid applications. The choice of method is, for instance, dependent on the purpose and performance of the final task and the possibility to put in time and effort in the creation of the grid application. Alchemi [22] is a part

of the GRIDBUS project [23] and is a .NET-based grid computing framework (grid middleware) that provides the runtime machinery and programming environment required to construct desktop grids and develop grid applications [23].

The purpose of applying the Grid-PEEC is to improve the performance of a 3D, quasi-static, frequency domain, PEEC-based EM solver capable of handling nonorthogonal structures. The original code is written in C++ and runs on a Windows environment. This type of code (quasi-static, Finite-Difference based, and nonorthogonal) was chosen since

- Quasi-static, frequency domain PEEC solvers operate on static partial elements with the multiplication of the phase shift at each frequency thus there is no need for recalculating the elements at each frequency (as for full-wave solvers) which simplifies the task.

- Nonorthogonal partial elements are time consuming to calculate and thus a considerable speed up could be expected. Consider the calculation of nonorthogonal partial inductances using a simple Gauss-Legendre quadrature. In the current code this takes 13 ms/inductance when using 5 weights for the length and width direction respectively and 2 weights in the thickness direction. For near couplings, 8th order Gauss-Legendre quadrature can be necessary increasing the time to 75 ms/inductance. Coefficients of potentials are somewhat faster to calculate since it is assumed that the charges to reside on the surface of the conductors converting a volume integral to a surface integral, as depicted in the previous section.

- To solve for each frequency point no history of previous voltages and currents are needed as for time domain solvers thus simplifying the task.

There are three grid applications created by the grid-PEEC program. The first one is the *Calculation of Coefficients of Potentials*, grid application two is the *Calculation of Partial Inductances*, and the third is the *Solution of Frequency Domain Problem*. The PEEC program will execute these grid applications one at a time starting with *Calculation of Coefficients of Potentials*, then in turn follows as the above mentioned order. The PEEC-program creates a thread that creates a grid application that sends the calculations out on the grid. The thread that started the grid application is in the meantime stopped/paused until its grid calculations is carried out. The choice of Alchemi in this grid application is based ,firstly, on the usage of the old code written in C++ without major modifications and, secondly, on the simplicity to setup and manage the grid application. The modified code works as follows:

1. Manager performs:

   - parsing and meshing,.
   - calculations of $\mathbf{A}$ and $\mathbf{R}$.
   - setup $\mathbf{I}_S$ and $\mathbf{V}$.
   - check how many executors.

2. Partition calculation of coefficients of potentials on the connected executors (fill **P**). Keep track of non-fill-ins.

3. Partition calculations of partial inductances on the connected executors (fill **L**). Keep track of non-fill-ins.

4. Solve Eq. (4.35) on the executors. Collect the results.

Results from the above applications show that the partial element calculation time is not improved by the grid-PEEC application but the frequency sweep time is clearly improved by this application.

4.4 Dyadic Green's Function, the Method of Complex Images and PEEC

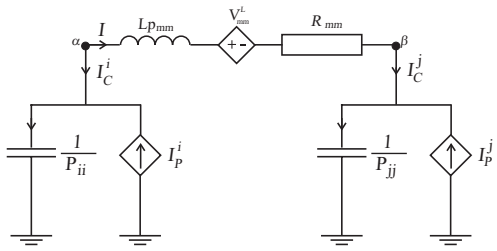

Figure 4.6: Basic PEEC building block for conducting wire.

In the PEEC method, the integral form of Maxwell's equations is interpreted as Kirchoff's voltage law applied to a basic PEEC cell which results in a complete circuit solution for 3D geometries, see Fig. 4.6 for the basic circuit. The equivalent circuit formulation allows for additional SPICE-type circuit elements to easily be included. Further, the models and the analysis apply to both the time and the frequency domain.

The circuit equations resulting from the PEEC model are easily constructed using a condensed modified loop analysis (MLA) or modified nodal analysis (MNA) formulation. In the MNA formulation, the volume cell currents and the node potentials are solved simultaneously for the discretized structure. To obtain field variables, post-processing of circuit variables are necessary.

Solving Maxwell's equations for systems which include a source above a dielectric surface desires application of the CIM and dyadic Green's functions. A dyad is a rank two tensor that can be represented as a matrix. Hence, a multiplication of a vector $\vec{A}$

and the dyad $\overline{\overline{D}}$ can be represented as

$$\overline{\overline{D}}\vec{A} = \begin{bmatrix} D_{11} & D_{12} & D_{13} \\ D_{21} & D_{22} & D_{23} \\ D_{31} & D_{32} & D_{33} \end{bmatrix} \begin{bmatrix} A_1 \\ A_2 \\ A_3 \end{bmatrix} \tag{4.36}$$

A dyad may be represented as a pair of vectors without any sign between and a (3×3) dyad is represented as a linear combination of three of such dyads as

$$\overline{\overline{D}} = \vec{A}\vec{B} + \vec{P}\vec{Q} + \vec{R}\vec{S} \tag{4.37}$$

Multiplication between vectors and dyads is defined such that a product of the identity dyad $\overline{\overline{I}} = \hat{x}\hat{x} + \hat{y}\hat{y} + \hat{z}\hat{z}$ and any vector $\vec{V}$ yields the vector itself, that is

$$\begin{aligned} \overline{\overline{I}} \cdot \vec{V} &= (\hat{x}\hat{x} + \hat{y}\hat{y} + \hat{z}\hat{z}) \cdot (v_1\hat{x} + v_2\hat{y} + v_3\hat{z}) \\ &= \hat{x}v_1 + \hat{y}v_2 + \hat{z}v_3 \\ &= \vec{V} \end{aligned} \tag{4.38}$$

The electric field $\bar{E}$ for a layered medium is a three-dimensional convolution between the dyadic Green's function and the source current density $\bar{J}$. This convolution integral is strongly singular which makes the numerical integration very time-consuming. Solving this type of integral is one of the topics within electromagnetism. By using the CIM, the appropriate Green's function is obtained much easier in terms of, for instance, spherical wave components where the real and imaginary sources are expressed in a series of summations [24, 3]. As a result, the time complexity for computing coefficients of potential P_{ij} and partial inductances Lp_{ij} within PEEC is improved. The appropriate Green's functions, obtained in this process, will also be used to determine the volume cell currents I and node voltages V in a structure.

Electric and magnetic field of an electric dipole in the vicinity and within an infinite perfect electric conductor (PEC)- or dielectric plane are subjects that can be studied and facilitated by applying the image methods (IM) and the complex image methods (CIM). For a layered medium, the idea of the CIM is to transform the problem into a combination of the source dipole and image dipoles with real and complex locations in space and in the absence of the layered medium, see Fig. 4.7. The radiation dyadic integral is expressed as

$$\bar{E}(\vec{r}, \omega) = -j\omega\mu \left[\overline{\overline{I}} + \frac{1}{\beta^2}\right] \int \overline{\overline{G}}(\vec{r}, \vec{r}')d\vec{r}' \tag{4.39}$$

where ω and μ are the angular frequency and the magnetic characteristic, respectively. $\vec{r}$ is the observation point distance to the origin and $\vec{r}'$ is the distance from the origin to the source point. The identity dyad $\overline{\overline{I}}$ is defined as $\overline{\overline{I}} = \hat{x}\hat{x} + \hat{y}\hat{y} + \hat{z}\hat{z}$. The radiation integral in (4.39) gives the solution of the Maxwell's equations in terms of a Green's function

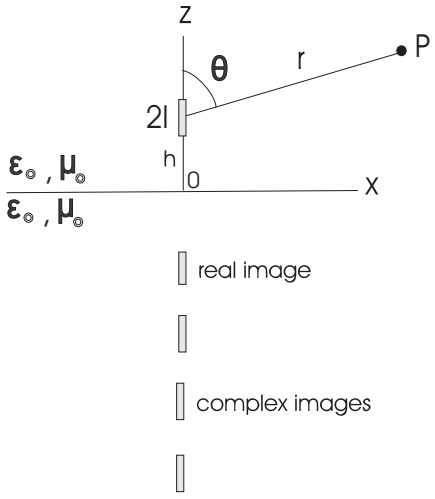

Figure 4.7: Real and complex images for a vertical dipole above a dielectric plane.

formulation. The Green's function in this case will be a 3×3 matrix of functions, or dyadic as

$$\overline{\overline{G}} = \left[\overline{\overline{I}} + \frac{1}{\beta^2}\nabla\nabla\right] \frac{e^{j\beta|\vec{r}-\vec{r}'|}}{4\pi|\vec{r}-\vec{r}'|} \tag{4.40}$$

The integral in (4.39) is strongly singular which makes the numerical integration very time-consuming. As mentioned earlier, solving this type of integral is one of the topics within electromagnetism. For the case of an infinitesimal vertical dipole above a dielectric half-plane, (4.39) can be rewritten as

$$E_z(z) = \frac{1}{j\omega\epsilon_0} \int_{z'} \left(\beta_0^2 + \frac{\partial^2}{\partial z^2}\right) G_A^{zz} I(z')dz' \tag{4.41}$$

where β_0 is the free-space wave-number and G_A^{zz} is the dyadic Green's function for the vector potential A. It is shown that the dyadic Green's function in the above equation takes the form of a Sommerfeld-type integral for an infinitesimal vertical dipole located at (x', y', z') above a dielectric half-space with the relative permittivity ϵ_r [25]. This is an slowly convergent integral which is cumbersome to solve numerically. However, by complex image methods, as it is illustrated in Fig. 4.7 this dyadic Green's function can be solved much easier in terms of spherical wave components as [24]

$$G_A^{zz} = \frac{e^{-j\beta_0 R_s}}{4\pi R_s} - K\frac{e^{-j\beta_0 R_q}}{4\pi R_q} + \sum_{i=1}^{N} \frac{e^{-j\beta_0 R_i}}{4\pi R_i} \quad , N = 3 \sim 5 \tag{4.42}$$

where $K = (1-\epsilon_r)/(1+\epsilon_r)$, and R_s, R_q, and R_i are distances from the source point, real image point (quasidynamic image), and i-th image respectively to the field point.

Coefficients of potential and partial inductances for a layered medium can generally be determined by [26]

$$P_{ij} = \frac{A_i}{4\pi\epsilon} \int_{S_j} G_\phi(r_{c_i}, r')dr' \tag{4.43}$$

and

$$L_{ij} = \frac{\mu}{4\pi} \int_{V_i} \int_{V_j} G_A(r, r')\hat{l}_j\hat{l}_i dr'dr \tag{4.44}$$

respectively, where G_ϕ and G_A are the scalar Green's function and the vector Green's function. V and S are the union of conductor volumes and surfaces; $\hat{l} = [l_x, l_y, l_z]$ is the direction in which a constant current density flows; the associated volume current and the surface charge of the conductor are approximated so that the discretized conductor volumes are assumed to be short and thin by a finite length and a cross sectional area. The conductor surfaces are also discretized into small panels each by a small area S and a centroid location r_c. For a layered medium, G_A, i.e. the vector Green's function, is defined as

$$G_A = \begin{bmatrix} G^A_{xx} & 0 & 0 \\ 0 & G^A_{yy} & 0 \\ G^A_{xz} & G^A_{yz} & G^A_{zz} \end{bmatrix} \tag{4.45}$$

where the matrix elements will be determined by the method of the complex images by definition of $\vec{r}' = [x', y', z']$ as a vector from the origin to the source point. For the free-space, $\vec{r} = [x, y, z]$ and for a real image, $\vec{r} = [x, y, -z]$. For a complex image, $\vec{r} = [x, y, -z + jb]$ where the real b will be determined by, for example, Prony's method [3][4].
Based on the PEEC method, the coefficients of potential are obtained by

$$p_{ij} = \frac{1}{S_i S_j \epsilon} \int_{S_j} \int_{S_i} G(\vec{r}_i, \vec{r}_j)dS_j dS_i \tag{4.46}$$

where S_i and S_j are the surface areas of cell i and j, created in the PEEC discretization. The Green's function in the above case, i.e. in the case of a vertical dipole above a PEC plane, is shown to be [24] $G = G_{free-space} - G_{image}$ where

$$G_{free-space} = \frac{1}{4\pi|\bar{r}_i - \bar{r}_j|}, \quad G_{image} = \frac{1}{4\pi|\bar{r}_i - \bar{r}_q|} \tag{4.47}$$

in which $|\bar{r}_i - \bar{r}_j|$ and $|\bar{r}_i - \bar{r}_q|$ represent respectively the distances to the field point from the source point and to the quasi-dynamic image, i.e. the distance between the source point and its classical real image. This means that each element in the matrix for partial element potential coefficients p_{ij} includes the subtraction $G_{free-space} - G_{image}$.

Determining of the total partial self- and mutual inductances for a structure above a PEC plane will be analogous to that of the partial coefficients of potential [27], that is

$$L_{total} = L_{free-space} - L_{image} \tag{4.48}$$

where the elements in the matrix $L_{free-space}$ are the partial self- and mutual inductances for the physical segments; L_{image} is the matrix including partial mutual inductances between the physical segments and their images.

Based on the coupled formulation of the PEEC method and CIM, a so-called Z-section test was done where the system was consisted of two rails, a ground plane, and a discontinuity, see Fig. 4.8. The computational time was considerably reduced by approximating the ground effects and the reduced number of unknowns, in comparison to the case where the ground were gridded. Some of the case studies showed computational

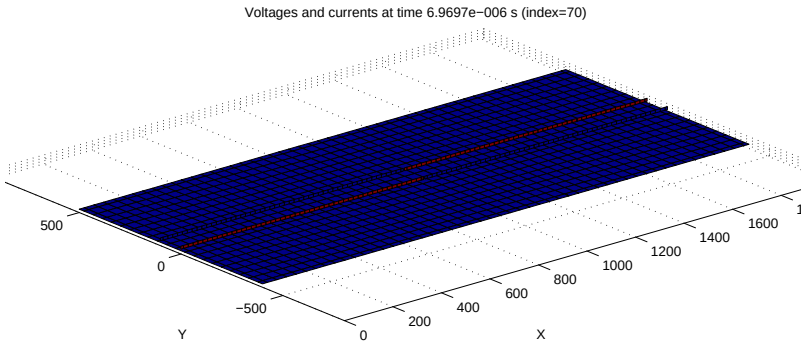

Figure 4.8: Voltages and currents in a Z-section test .

speed ups for EM problems containing large ground planes where the PEEC method and the CIM were applied. These results are as follows:

- In the case of the PIFA test from paper A, the frequency domain, quasi-static solution by 100 steps and gridded ground plane resulted into $585 + 322$ unknowns. This was solved by regular PEEC in 1 minute, 44 seconds. Removed ground plane resulted into $155 + 91$ unknowns by the solution time of 3 seconds.

- In the case of the Z-section test, mentioned in Chapter 4, the frequency domain, quasi-static solution by 100 steps and gridded ground plane resulted in $2270 + 1275$ unknowns. This was solved by regular PEEC in 56 minutes. Removed ground plane resulted in $200 + 204$ unknowns. This was solved in 5 seconds.

It should be mentioned that the speed ups were strongly application dependent.

Chapter 5

Paper Summaries

In this chapter, summaries of two conference contributions are presented.

5.1 Paper A: Antenna Analysis Using PEEC and the Complex Image Method

The PEEC method is a 3D, full wave modeling method suitable for combined electromagnetic and circuit analysis. In the PEEC method, the integral equation is interpreted as Kirchoff's voltage law applied to a basic PEEC cell which results in a complete circuit solution for 3D geometries. The equivalent circuit formulation allows for additional SPICE-type circuit elements to easily be included. Further, the models and the analysis apply to both the time and the frequency domain.

The circuit equations resulting from the PEEC model are easily constructed using a condensed modified loop analysis (MLA) or modified nodal analysis (MNA) formulation. In the MNA formulation, the volume cell currents and the node potentials are solved simultaneously for the discretized structure. To obtain field variables, post-processing of circuit variables is necessary.

In this paper, it is shown that how the PEEC method is applied to model antenna characteristics, including input impedance and radiation diagrams, by use of the appropriate Green's function in the calculation of partial elements. The electric field for a layered medium is a three-dimensional convolution between the dyadic Green's function and the source current density. This convolution integral is strongly singular which makes the numerical integration very time-consuming. Solving this type of integral is one of the topics within electromagnetism. By using the complex image method (CIM), the appropriate Green's function is obtained much easier in terms of, for instance, spherical wave components where the real and imaginary sources are expressed in a series of summations. As a result, the time complexity for computing coefficients of potential P_{ij} and partial inductances Lp_{ij} within PEEC is improved. The appropriate Green's functions, obtained in this process, will also be used to determine the volume cell currents I and node voltages V in a structure.

5.2 Paper B: Optimization of PEEC Based Electromagnetic Modeling Code Using Grid Computing

Different speed-up approaches for PEEC have been presented by, for instance, using wavelet transform and fast multipole method . This paper presents a grid based approach with the potential of speeding up both partial element computations and the solution of the resulting equation system. Therefore, three different grid applications are created by a grid-PEEC program which handles the calculation of coefficients of potentials, the calculation of partial inductances, and the solution of the frequency domain circuit equations.

This paper deals with the optimization of an existing frequency domain, nonorthogonal partial element equivalent circuit based electromagnetic analysis code using the freeware Alchemi toolkit in a Windows environment. The purpose is to speed up both the calculation of the nonorthogonal partial elements and the solution of the frequency

domain systems. To enable satisfactory results, construction of a linear algebra library was required. The original PEEC code uses the Matrix TCL Pro 2.12 and a complex linear algebra library.

Chapter 6

Conclusions and Further Work

6.1 Conclusions

The main objective of this thesis has been to reduce the computational time for numerically large problems, resembling the railway system in which numerical solution of the electromagnetic modeling has been a bottleneck, due to the ground effects. To deal with this complication, the image methods and complex image methods were applied to different structures above a PEC surface by infinite extent. Results of the case studies showed a radical reduction in computational time, see results in Ch. 4.4. In these case studies, the PEEC method and complex image methods were applied. For nonorthogonal structures, grid-computing technology was applied to optimize a 3D, quasi-static, frequency domain PEEC-based EM-solver. By this technology, the calculation time results for the partial elements could not be improved but the solution time for the frequency domain systems were considerably reduced, see Paper B.

Although the solved problems had an idealized nature, a huge amount of computational memory was used which implies that the PEEC-based electromagnetic field solution is expected to rely more on parallel algorithms in circumstances where the access to super computers is limited. The electromagnetic modeling will be a completion to EMC tests to constitute an indicator when maintaining of the railway system. In order to the radical improvement of these electromagnetic calculations by these methods, it will be possible to design a more developed maintenance program in which EMC, as a whole, constitutes an indicator within railway maintenance.

6.2 Further work

Further work will include a robust implementation of the theory presented here. Then, extensive testing of the improvement, firstly on problems with large ground plane and secondly on problems with large planes of dielectric material is needed. In future work and in the railway applications, the ground should be assumed as a dielectric medium which requires naturally more complicated electromagnetic modeling. A combination of complex image methods and grid computing technology will, in this case, be applicable in order to electromagnetic modeling of the ground as a dielectric media and as a numerically large system.

The combination of PEEC and CIM can further be applied to analysis of other layered media, for example, printed circuit boards.

References

[1] Juan R. Mosig, "Arbitrary shaped Microstrip structures and Their analysis with a Mixed Potential Integral Equation", *IEEE Trans. on Microwaves Theory Tech.*, vol. MTT-36, pp. 314-323, Feb. 1988.

[2] W. C. Chew, *Waves and Fields in Inhomogeneous Media.* New York: IEEE PRESS Series on Electromagnetic Waves, 1995.

[3] J. J. Yang, Y. L. Chow, D. G. Fang, "Discrete complex images of a three-dimonsional dipole above and within a lossy ground", *IEE Proceedings-H*, vol. 138, No. 4, Aug. 1991.

[4] F. B. Hildebrand, *Introduction to Numerical Analysis*, Second Edition, Dover Publications, Inc., New York, 1987.

[5] C Britsman, ÅL., S O Ottosson, *Handbook i FMEA*, Produktion: Ord & Form AB, Uppsala 1993.

[6] Andrew Rowell, "Ensuring Compliance with European and International Standards and Regulations", York EMC Services Ltd, University of York, UK, March 2005.

[7] Andrew Rowell, "EMC Measurements & Environments", York EMC Services Ltd, University of York, UK, March 2005.

[8] *Railway applications - Electromagnetic compatibility, Part 2: Emission of the whole railway system to the outside world:* SS-EN 50121-2, SIS (Swedish Institute of Standards), 2000.

[9] M. N. O. Sadiku, *Numerical Techniques in Electromagnetics.* CRC Press, Inc. 1992.

[10] Gunnar Sparr, *Kontinuerliga System*, Lund Institute of Technology, Department of Mathematics, Sweden. Lund 1984.

[11] George B. Arfken, Hans J. Weber, *Mathematical Methods for Physicists*, Academic Press, 2001.

[12] D. K. Cheng, *Field and Wave Electromagnetics.* Addison-Wesley Publishing Co., Reading, Mass., 1989.

[13] D. K. Cheng, *Fundamentals of Engineering Electromagnetics.* Addison-Wesley Series in Electrical Engineering, Nov. 1993.

[14] C. A. Balanis, *Antenna Theory: Analysis and Design.* John Wiley & Sons, Inc., 1982.

[15] C. A. Balanis, *Advanced Engineering Electromagnetics.* John Wiley & Sons, Inc., 1989.

[16] J. Ekman, "Electromagnetic Modeling Using the Partial Element Equivalent Circuit Method", Ph.D. dissertation, Luleå University of Technology, 2003.

[17] A. E. Ruehli, "Circuit Models for Three-Dimensional Geometries Including Dielectrics", *IEEE Trans. Microwave Theory Tech.*, vol. 40, no. 7, pp. 1507–1516, Jul. 1992.

[18] C. Ho, A. Ruehli, and P. Brennan, "The Modified Nodal Approach to Network Analysis", *IEEE Trans. Circuits Syst.*, pp. 540–509, Jun. 1975.

[19] A. E. Ruehli *et al.*, "Nonorthogonal PEEC Formulation for Time- and Frequency-Domain EM and Circuit Modeling", *IEEE Trans. on EMC*, vo. 45, no. 2, pp. 167-176, May 2003.

[20] A. E. Ruehli, "Equivalent Circuit Models for Three-Dimensional Multiconductor Systems", *IEEE Trans. Microwave Theory Tech.*, vl. 22, no. 3, pp. 216–221, Mar. 1974.

[21] J. E. Garrett, "Advancements of the Partial Element Equivalent Circuit Formulation", PhD dissertation, The University of Kentucky, 1997.

[22] Alchemi [.NET Grid Computing Framework] Homepage (2005-05-17). [Online]. Available: http://www.alchemi.net/

[23] Grid Computing and Distributed Systems (GRIDS) Laboratory Homepage (2005-05-17). [Online]. Available: http://www.gridbus.org/

[24] R. M. Shubair and Y. L. Chow, "A Closed Form Solution of Vertical Dipole Antennas above a Dielectric Half-Space", *IEEE Tran. on Antenna and Prop.*, Dec., 1993.

[25] A. Banos, *Dipole Radiation in the Presence of a Conducting Half Space*, New York: Pergamon, p. 35, 1969.

[26] Xin Hu, Jacob White, Jong Hoon Lee, Luca Daniel, "Analysis of Full-wave Conductor System Impedance over Substrate Using Novel Integration Techniques." DAC 2005, June 13-17, 2005, Anaheim, California, USA.

[27] Daniel Melendy, Andreas Weisshar, "A New Scalable Model for Spiral Inductors on Lossy Silicon Substrate", Oregon State University, Department of Electrical and Computer Engineering, 2003.

Part II

Paper A

Antenna Analysis Using PEEC and the Complex Image Method

Authors:
Farid Monsefi and Jonas Ekman, Department of Computer Science and Electrical Engineering, Luleå University of Technology, Sweden

Reformatted version of paper originally published in:
The Nordic Antenna Symposium, 30 May - 1 June 2006, Linköping, Sweden.

Antenna Analysis Using PEEC and the Complex Image Methods

Farid Monsefi and Jonas Ekman, Department of Computer Science and Electrical Engineering, Luleå University of Technology, Sweden

Abstract

The partial element equivalent circuit (PEEC) method has been developed from VLSI inductance calculations in the early 70s. The method is still evolving and new application areas are continuously reported. In this paper we show how the PEEC method is utilized to model antenna characteristics by the use of the appropriate Green's functions. By applying the complex image methods due to a layered medium, the potential, generated by a source, will be the same as the sum of potentials by a combination of the source itself and image sources including both real and image locations. Calculated and analytical results are compared for dipoles while more complex antenna designs are compared with published results by other researchers. Fast and accurate results encourage for further work.

1 Introduction

Image methods are applied within antenna theory to give an equivalent system near an infinite plane conductor or dielectric where there exists symmetry in the geometry of the problem [1]. In this paper, it will be shown that how the PEEC method [2, 3] is utilized to model antenna characteristics, including input impedance and radiation diagrams, by use of the appropriate Green's function in the calculation of partial elements. The electric field $\bar{E}$ for a layered medium is a three-dimensional convolution between the dyadic Green's function and the source current density $\bar{J}$. This convolution integral is strongly singular which makes the numerical integration very time-consuming. Solving this type of integral is one of the topics within electromagnetism. By using the complex image methods (CIM), the appropriate Green's function is obtained much easier in terms of, for instance, spherical wave components where the real and imaginary sources are expressed in a series of summations [4, 5]. As a result, the time complexity for computing coefficients of potential P_{ij} and partial inductances Lp_{ij} within PEEC is improved. The appropriate Green's functions, obtained in this process, will also be used to determine the volume cell currents I and node voltages V in a structure.

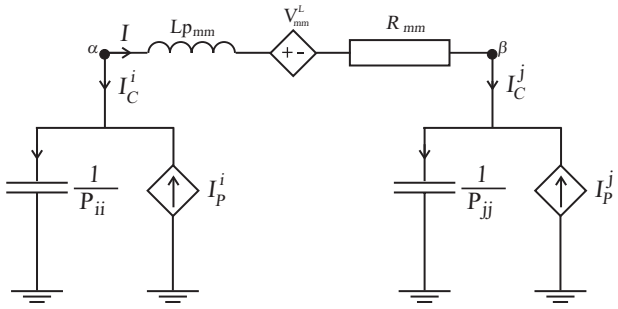

Figure 1: Basic PEEC building block for conducting wire.

2 Basic PEEC Theory

The PEEC method is a 3D, full wave modeling method suitable for combined electromagnetic and circuit analysis. In the PEEC method, the integral equation is interpreted as Kirchoff's voltage law applied to a basic PEEC cell which results in a complete circuit solution for 3D geometries, see Fig. 1 for the basic circuit. The equivalent circuit formulation allows for additional SPICE-type circuit elements to easily be included. Further, the models and the analysis apply to both the time and the frequency domain. The circuit equations resulting from the PEEC model are easily constructed using a condensed modified loop analysis (MLA) or modified nodal analysis (MNA) formulation. In the MNA formulation, the volume cell currents and the node potentials are solved simultaneously for the discretized structure. To obtain field variables, post-processing of circuit variables are necessary.

3 Image Methods and Complex Image Methods

Electric and magnetic field of an electric dipole in the vicinity and within an infinite perfect electric conductor (PEC)- or dielectric plane are subjects that can be studied and facilitated by applying the image methods (IM) and the complex image methods (CIM) [4][5]. Due to a layered medium, the idea of the CIM is to transform the problem into a combination of the source dipole and image dipoles with real and complex locations in space and in the absence of the layered medium, see Fig. 2. The radiation dyadic integral is expressed as

$$\bar{E}(\vec{r},\omega) = -j\omega\mu \left[\overline{\overline{I}} + \frac{1}{\beta^2}\right] \int \overline{\overline{G}}(\vec{r},\vec{r}')d\vec{r}' \tag{1}$$

where ω and μ are the angular frequency and permeability, respectively. $\vec{r}$ is the observation point distance to the origin and $\vec{r}'$ is the distance from the origin to the source point. The identity dyad $\overline{\overline{I}}$ is defined as $\overline{\overline{I}} = \hat{x}\hat{x} + \hat{y}\hat{y} + \hat{z}\hat{z}$. The radiation integral in (1) gives the solution of the Maxwell's equations in terms of a Green's function formulation.

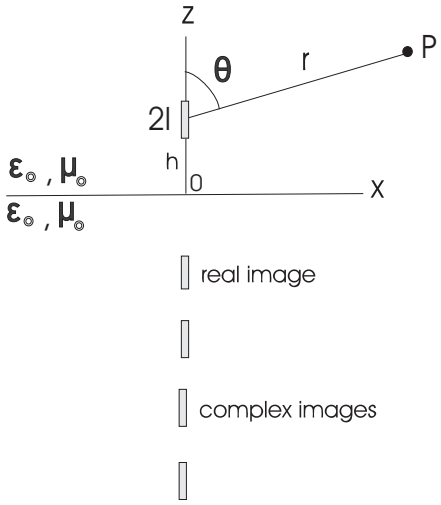

Figure 2: Real and complex images for a vertical dipole above a dielectric plane.

The Green's function in this case will be a 3×3 matrix of functions, or dyadic as

$$\overline{\overline{G}} = \left[\overline{\overline{I}} + \frac{1}{\beta^2}\nabla\nabla\right] \frac{e^{j\beta|\vec{r}-\vec{r}'|}}{4\pi|\vec{r}-\vec{r}'|} \tag{2}$$

The integral in (1) is strongly singular which makes the numerical integration very time-consuming. Solving this type of integral is one of the topics within electromagnetism. For the case of an infinitesimal vertical dipole above a dielectric half-plane, (1) can be rewritten as

$$E_z(z) = \frac{1}{j\omega\epsilon_0}\int_{z'}\left(\beta_0^2 + \frac{\partial^2}{\partial z^2}\right) G_A^{zz} I(z')dz' \tag{3}$$

where β_0 is the free-space wave-number and G_A^{zz} is the dyadic Green's function for the vector potential A. It is shown that the dyadic Green's function in the above equation takes the form of a Sommerfeld-type integral for an infinitesimal vertical dipole located at (x', y', z') above a dielectric half-space of the relative permittivity ϵ_r [6]. This is an slowly convergent integral which is cumbersome to solve numerically. However, by complex image methods, as it is illustrated in Fig. 2 this dyadic Green's function can be solved much easier in terms of spherical wave components as [4]

$$G_A^{zz} = \frac{e^{-j\beta_0 R_s}}{4\pi R_s} - K\frac{e^{-j\beta_0 R_q}}{4\pi R_q} + \sum_{i=1}^{N}\frac{e^{-j\beta_0 R_i}}{4\pi R_i} \quad , N = 3 \sim 5 \tag{4}$$

where $K = (1-\epsilon_r)/(1+\epsilon_r)$, and R_s, R_q, and R_i are distances from the source point, real image point (quasidynamic image), and i-th image respectively to the field point.

The classical image solution of an infinitesimal vertical dipole above a PEC plane can be derived where the third term in (4) is vanished. This Green's function is

$$G_A^{zz} = \frac{e^{-j\beta_0 R_s}}{4\pi R_s} - \frac{e^{-j\beta_0 R_q}}{4\pi R_q} \tag{5}$$

By applying image methods, the input impedance of a horizontal dipole above a PEC plane, as described in [1], can be calculated as a summation of self- and mutual impedances. For determining the input impedance for a horizontal dipole located above a PEC plane, a side-by-side configuration can be applied. For this case, the self-impedance Z_{11} will be computed as $Z_{11} = R_{11} + jX_{11}$ where R_{11} and X_{11} are input- resistance and reactance. The mutual impedance for a side-by-side dipole configuration is computed as $Z_{21} = R_{21} + jX_{21}$ where R_{21} and X_{21} are the mutual- resistance and reactance. This computation of the input impedance is based on the current at the input.

4 Combining PEEC and CIM

Coefficients of potential and partial inductances as calculated in the PEEC method, for a layered medium are generally determined by [7]

$$P_{ij} = \frac{A_i}{4\pi\epsilon} \int_{S_j} G_\phi(r_{c_i}, r')dr' \tag{6}$$

respectively

$$L_{ij} = \frac{\mu}{4\pi} \int_{V_i} \int_{V_j} G_A(r, r')\hat{l}_j \hat{l}_i dr' dr \tag{7}$$

where G_ϕ and G_A are the scalar Green's function and the vector Green's function. V and S are the union of conductor volumes and surfaces; $\hat{l} = [l_x, l_y, l_z]$ is the direction in which a constant current density flows; the associated volume current and the surface charge of the conductor are approximated so that the discretized conductor volumes are assumed to be short and thin by a finite length and a cross sectional area. The conductor surfaces are also discretized into small panels each by a small area S and a centroid location r_c. For a layered medium, G_A, i.e. the vector Green's function, is defined as

$$G_A = \begin{bmatrix} G_{xx}^A & 0 & 0 \\ 0 & G_{yy}^A & 0 \\ G_{xz}^A & G_{yz}^A & G_{zz}^A \end{bmatrix} \tag{8}$$

where the matrix elements will be determined by the method of the complex images by definition of $\vec{r}' = [x', y', z']$ as a vector from the origin to the source point. For the free-space, $\vec{r} = [x, y, z]$ and for a real image, $\vec{r} = [x, y, -z]$. For a complex image, $\vec{r} = [x, y, -z + jb]$ where the real b will be determined by, for example, Prony's method

[5]. The induced electric field for an infinitesimal vertical dipole (or PEEC model volume cell) above a PEC plane, see Fig. 2, due to far-field observation is [1]

$$E_\theta = j\eta \frac{\beta I_0 l e^{-j\beta\vec{r}}}{4\pi r} sin\theta \left[2cos\left(\beta h \cos\theta\right)\right] \tag{9}$$

where h is the vertical distance between the PEC plane and the closest end of the dipole, l is the length of the dipole, and I_0 is the constant electric current. Further, θ is the angle between z-axis and $\vec{r}$ which is the radial distance between the original of the coordinate system and the observation point. An equivalent formulation can be used where the dipole is divided into N infinitesimal vertical dipoles, located along the positive z-axis. The far-zone electric field, caused by contribution from all of these infinitesimal vertical dipoles, can be written as

$$E_\theta^n \simeq \sum_{n=1}^{N} j\eta \frac{\beta I_0^{(n)} l_n e^{-j\beta\vec{r}}}{4\pi r} \sin\theta \times \{2\cos[(h + \frac{2n-1}{2} l_n)\beta\cos\theta]\} \tag{10}$$

for $z > 0$. The strategy is to mesh structures according to PEEC method where the length l_n of the cell n coincides with an appropriate infinitesimal vertical dipole along one axis. I_0^n, is the volume cell currents give by the PEEC solver using the partial elements from (6) and (7).

4.1 Partial Element Calculations Applying PEEC and IM

Based on the PEEC method, the coefficients of potential are obtained by

$$p_{ij} = \frac{1}{S_i S_j \epsilon} \int_{S_j} \int_{S_i} G(\vec{r_i}, \vec{r_j}) dS_j dS_i \tag{11}$$

where S_i and S_j are the surface areas of cell i and j, created in the PEEC discretization. By application of (5), the Green's function in the above case, i.e. in the case of a vertical dipole above a PEC plane, is shown to be [4] $G = G_{free-space} - G_{image}$ where

$$G_{free-space} = \frac{1}{4\pi|\bar{r}_i - \bar{r}_j|}, \quad G_{image} = \frac{1}{4\pi|\bar{r}_i - \bar{r}_q|} \tag{12}$$

in which $|\bar{r}_i - \bar{r}_j|$ and $|\bar{r}_i - \bar{r}_q|$ represent respectively the distances to the field point from the source point and to the quasidynamic image, i.e. the distance between the source point and its classical real image. This means that each element in the matrix for partial element potential coefficients p_{ij} includes the subtraction $G_{free-space} - G_{image}$. Determining of the total partial self- and mutual inductances for a structure above a PEC plane will be analogous to that of the partial coefficients of potential [8], that is

$$L_{total} = L_{free-space} - L_{image} \tag{13}$$

where the elements in the matrix $L_{free-space}$ are the partial self- and mutual inductances for the physical segments; L_{image} is the matrix including partial mutual inductances between the physical segments and their images.

5 Numerical Results

This section gives two examples for PEEC models utilizing the theory described in previous sections.

5.1 $\frac{\lambda}{2}$Dipoles

The first example is a horizontal, thin wire dipole of length 50 mm and radius 0.01 μm, located above a PEC-plane as studied in [9]. For numerical modeling, a PEEC-

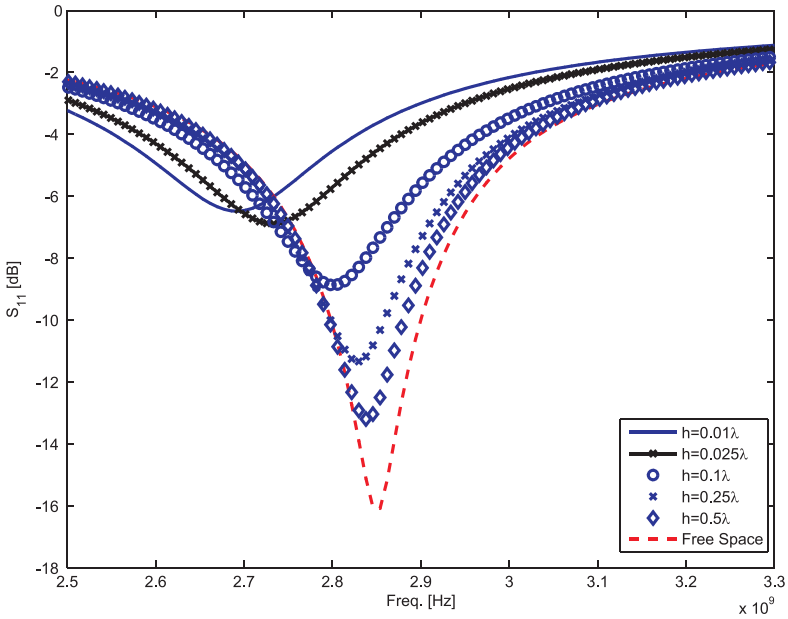

Figure 3: Resonance frequency results for a $\frac{\lambda}{2}$dipole above a PEC plane modeled using a combination of PEEC and IM.

based solver utilizing the modified computation of the partial elements from Chapter 4 to account for a PEC plane at $z = 0$ is used. Fig. 3 shows the computed driving point impedance of the dipole at various heights above the PEC-plane which compares well with the results from [9]. Fig. 4 shows the computed electric field strengths for two different heights above the PEC-plane. These results compare well with results from [1].

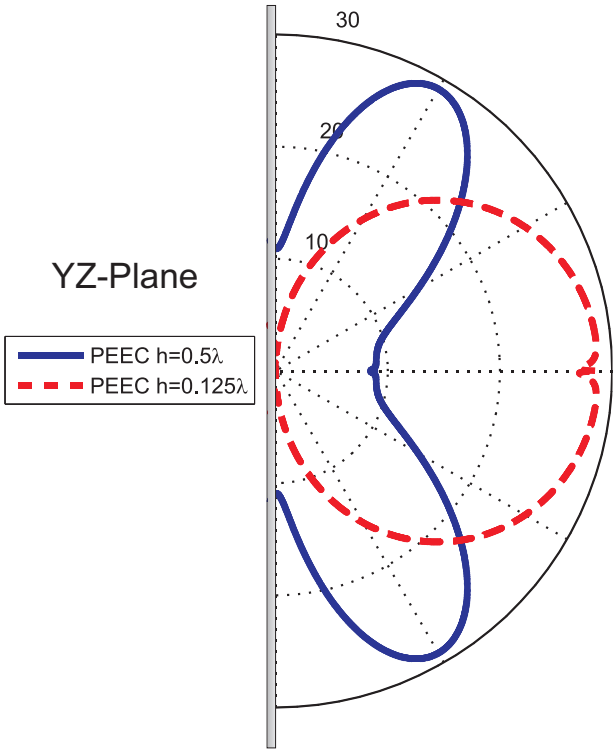

Figure 4: Electric field for different heights above a PEC-plane for a $\frac{\lambda}{2}$ dipole modeled using a combination of PEEC and IM.

5.2 Dual-band antenna (PIFA)

The second numerical example is the dual-band, PIFA antenna studied in [10]. The antenna consists of two interconnected, by an LC-trap, antenna elements (20 × 10 mm and 10 × 10 mm) above a PEC-plane. By using the traditional PEEC method, the antenna can be studied by modeling the PEC-plane. However, here we show the results by using the theory from above compared to a free-space situation (no PEC-plane). The PIFA-antenna is designed to have resonance frequencies around 900 and 1 800 MHz depending on the LC-trap. By using one of the suggested L-C-combination in [10], the Image-PEEC solver gives the result in Fig. 5. The resonance frequencies are 1 000 and 1 750 MHz without altering the L-C-combination which has to be considered well in comparison with the published results.

6 Conclusions and Discussion

In this work, we have shown that how image- and complex image methods can be combined with the partial element equivalent circuit (PEEC) method. The theory has been tested by inclusion in an existing PEEC solver and a few illustrative examples have been shown. For computing input impedance and the resonance frequency, there were small discrepancies between the already existing analytic solutions and the solutions which were given by the PEEC-image method. Further, the Green's functions which are obtained by both the image and the complex image method improve the computation time of the PEEC based solver by reducing the number of unknowns in the solution. Further work involves the study of infinite dielectric planes by using CIM and PEEC.

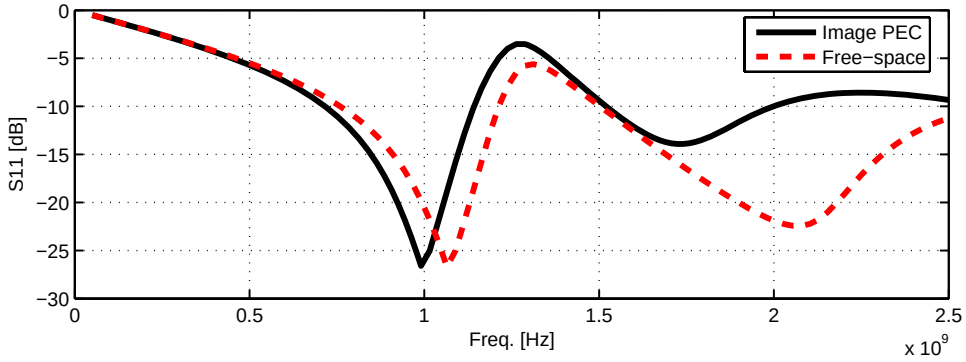

(a)

Figure 5: Resonance frequencies for a dual-band antenna (PIFA) above a PEC plane.

References

[1] C. A. Balanis, *Antenna Theory: Analysis and Design.* John Wiley & Sons, Inc., 1982.

[2] A. E. Ruehli, "Inductance calculations in a complex integrated circuit environment", *IBM Journal of Research and Development*, 16(5):470-481, September 1972.

[3] A. E. Ruehli and P. A. Brennan, "Efficient capacitance calculations for three-dimensional multiconductor systems", *IEEE Trans. on Microw. Theory and Tech.*, 21(2):76-82, February 1973.

[4] R. M. Shubair and Y. L. Chow, "A Closed Form Solution of Vertical Dipole Antennas above a Dielectric Half-Space", *IEEE Tran. on Antenna and Prop.*, Dec., 1993.

[5] J. J. Yang, Y. L. Chow, D. G. Fang, "Discrete complex images of a three-dimonsional dipole above and within a lossy ground", *IEE Proceedings-H*, vol. 138, No. 4, Aug. 1991.

[6] A. Banos, *Dipole Radiation in the Presence of a Conducting Half Space*, New York: Pergamon, p. 35, 1969.

[7] Xin Hu, Jacob White, Jong Hoon Lee, Luca Daniel, "Analysis of Full-wave Conductor System Impedance over Substrate Using Novel Integration Techniques." *DAC 2005, June 13-17, 2005, Anaheim, California, USA.*

[8] Daniel Melendy, Andreas Weisshar, "A New Scalable Model for Spiral Inductors on Lossy Silicon Substrate", Oregon State University, Department of Electrical and Computer Engineering, 2003.

[9] M. F: Abedin, and M. Ali, "Effects of EBG Reflection Phase Profiles on the Input Impedance and Bandwidth of Ultrathin Directional Dipoles", *IEEE Trans. on Ant. and Prop.*, vol. 53, No. 11, Nov. 2005.

[10] G. K. H. Lui and R. D. Murch, "Compact Dual-Frequency PIFA Designs Using LC Resonators", *IEEE Trans. on Ant. and Prop.*, 49(7):1016-1019, July 2001.

Paper B

Optimization of PEEC Based Electromagnetic Modeling Code Using Grid Computing

Authors:
Jonas Ekman and Farid Monsefi, Department of Computer Science and Electrical engineering , Luleå University of Technology, Sweden.

Reformatted version of paper originally published in:
The EMC Europe International Symposium on Electromagnetic Compatibility, 6-9 September 2006, Barcelona

Optimization of PEEC Based Electromagnetic Modeling Code Using Grid Computing

Jonas Ekman and Farid Monsefi, Department of Computer Science And Electrical engineering , Luleå University of Technology, Sweden.

Abstract

This papers deals with the optimization of an existing frequency domain, nonorthogonal partial element equivalent circuit based electromagnetic analysis code using the freeware Alchemi toolkit in a Windows environment. The purpose is to speed up both the calculation of the nonorthogonal partial elements and the solution of the frequency domain systems. The technology with this type of heterogeneous grid computing was shown to be very young and extensive work, including the construction of a linear algebra library, was required to enable satisfactory results.

1 Introduction

Partial element equivalent circuit (PEEC) models [1, 2, 3] are ideal for solving mixed circuit and electromagnetic problems. However, the newly introduced nonorthogonal PEEC formulation [4] is computationally demanding for partial element computations since semi-analytic computation routines can not be used. Worse case is for PEEC-based frequency domain, full-wave solvers which require the partial elements to be recomputed at each frequency step. Different speed-up approaches for PEEC have been presented by, for instance, using wavelet transform [5] and fast multipole method [6]. This paper presents a grid based approach with the potential of speeding up both partial element computations and the solution of the resulting equation system. Therefore, three different grid applications are created by a grid-PEEC program which handle the calculation of coefficients of potentials, the calculation of partial inductances, and the solution of the frequency domain circuit equations. Section 2 derives concisely the integral-based method of partial element equivalent circuit (PEEC). In Sec. 3, different kinds of software for grid computing are presented. The choice of method, which for instance, is dependent on the purpose and performance of the final task follows in this section. Also discussed is the possibility to put in time and effort in the creation of the grid application. The main purpose of this paper is handled in Sec. 4 where the attempt is to improve the performance of a 3D, quasi-static, frequency domain, PEEC-based EM-solver for nonorthogonal structures. Result for two test objects follows in Sec. 5. These are an orthogonal $\frac{\lambda}{2}$ dipole, and a nonorthogonal transmission line, respectively. Conclusions and discussion are found in Sec. 6.

2 Basic PEEC Theory

The PEEC method is a 3D, full wave modeling method suitable for combined electromagnetic and circuit analysis. In the PEEC method, the integral equation is interpreted as Kirchoff's voltage law applied to a basic PEEC cell which results in a complete circuit solution for 3D geometries. The equivalent circuit formulation allows for additional SPICE-type circuit elements to easily be included. Further, the models and the analysis apply to both the time and the frequency domain. The circuit equations resulting from the PEEC model are easily constructed using a condensed modified loop analysis (MLA) or modified nodal analysis (MNA) formulation [8]. In the MNA formulation, the volume cell currents and the node potentials are solved simultaneously for the discretized structure. To obtain field variables, post-processing of circuit variables are necessary. This section gives an outline of the nonorthogonal PEEC method as fully detailed in [4]. In this formulation, the objects, conductors and dielectrics, can be both orthogonal and nonorthogonal quadrilateral (surface) and hexahedral (volume) elements. The formulation utilizes a global and a local coordinate system where the global coordinate system uses orthogonal coordinates x, y, z where a global vector $\vec{F}$ is of the form $\vec{F} = F_x\vec{x} + F_y\vec{y} + F_z\vec{z}$. A vector in the global coordinates are marked as $\vec{r_g}$. The local coordinates a, b, c are used to separately represent each specific possibly non-orthogonal object and the unit vectors are $\vec{a}$, $\vec{b}$, and $\vec{c}$, see further [4]. The starting point for the theoretical derivation is the total electric field at a conductor expressed as

$$\vec{E}^i(\vec{r_g}, t) = \frac{\vec{J}(\vec{r_g}, t)}{\sigma} + \frac{\partial \vec{A}(\vec{r_g}, t)}{\partial t} + \nabla\phi(\vec{r_g}, t), \tag{1}$$

where $\vec{E}^i$ is the incident electric field, $\vec{J}$ is the current density in a conductor, $\vec{A}$ is the magnetic vector potential, ϕ is the scalar electric potential, and σ the electrical conductivity. The dielectric areas are taken into account as an excess current with the scalar potential using the volumetric equivalence theorem. By using the definitions of the vector potential $\vec{A}$ and the scalar potential ϕ we can formulate the integral equation for the electric field at a point $\vec{r_g}$ which is to be located either inside a conductor or inside a dielectric region according to

$$\begin{aligned} \vec{E}^i(\vec{r_g}, t) = & \frac{\vec{J}(\vec{r_g}, t)}{\sigma} \\ & + \mu \int_{v\prime} G(\vec{r_g}, \vec{r_g}\prime) \frac{\partial \vec{J}(\vec{r_g}\prime, t_d)}{\partial t} dv\prime \\ & + \epsilon_0(\epsilon_r - 1)\,\mu \int_{v\prime} G(\vec{r_g}, \vec{r_g}\prime) \frac{\partial^2 \vec{E}(\vec{r_g}\prime, t_d)}{\partial t^2} \\ & + \frac{\nabla}{\epsilon_0} \int_{v\prime} G(\vec{r_g}, \vec{r_g}\prime) q(\vec{r_g}\prime, t_d) dv\prime. \end{aligned} \tag{2}$$

Eq. (2) is the time domain formulation which can easily be converted to the frequency domain by using the Laplace transform operator $s = \frac{\partial}{\partial t}$ and where the time retardation

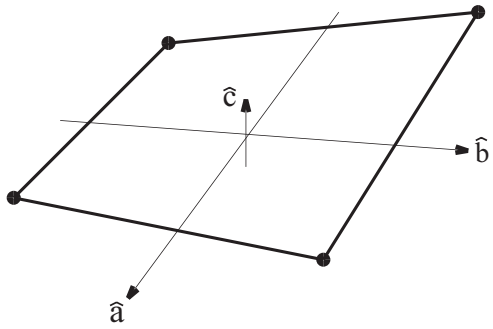

Figure 1: Nonorthogonal element created by the mesh generator with associated local coordinate system.

τ will transform to $e^{-s\tau}$. The PEEC integral equation solution of Maxwell's equations is based on the total electric field, e.g. (1). An integral or inner product is used to reformulate each term of (2) into the circuit equations. This inner product integration converts each term into the fundamental form $\int \vec{E} \cdot dl = V$ where V is a voltage or potential difference across the circuit element. It can be shown how this transforms the sum of the electric fields in (1) into the Kirchoff Voltage Law (KVL) over a basic PEEC cell [3]. Fig. 2 details the (L_p,P,τ)PEEC model for the metal patch in Fig. 1 when discretized using four edge nodes (dark full circles). The model in Fig. 2 consists of:

- partial inductances (L_p) which are calculated from the volume cell discretization using a double volume integral.
- coefficients of potentials which are calculated from the surface cell discretization using a double surface integral.
- retarded current controlled current sources, to account for the electric field couplings, given by $I_p^i = \frac{p_{ij}}{p_{ii}} I_C^j(t - t_{d_{ij}})$ where $t_{d_{ij}}$ is the free space travel time (delay time) between surface cells i and j,
- retarded current controlled voltage sources, to account for the magnetic field couplings, given by $V_L^n = Lp_{nm} \frac{\partial I_m(t-t_{d_{nm}})}{\partial t}$, where $t_{d_{nm}}$ is the free space travel time (delay time) between volume cells n and m.

By using the MNA method, the PEEC model circuit elements can be placed in the MNA system matrix during evaluation by the use of correct matrix stamps [8]. The MNA system, when used to solve frequency domain PEEC models, can be schematically described as

$$\begin{array}{rcl} j\omega \boldsymbol{P}^{-1} V - \boldsymbol{A}^T I & = & I_s \\ \boldsymbol{A} V - (\boldsymbol{R} + j\omega \boldsymbol{L}_p) I & = & V_s \end{array} \tag{3}$$

where: $\boldsymbol{P}$ is the coefficient of potential matrix, $\boldsymbol{A}$ is a sparse matrix containing the connectivity information, $\boldsymbol{L}_p$ is a dense matrix containing the partial inductances, elements

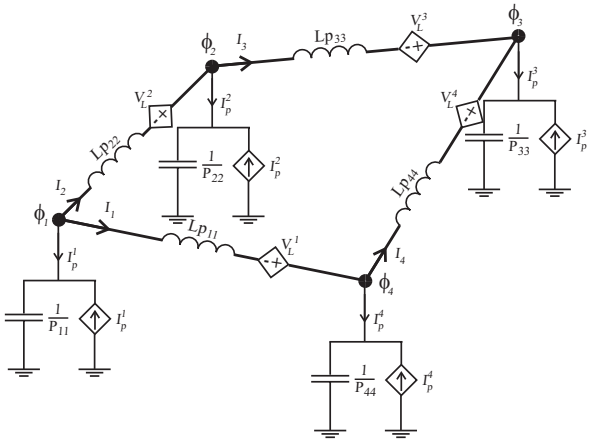

Figure 2: (L_p,P,τ)PEEC model for metal patch in Fig. 1 discretized with four edge nodes. Controlled current sources, I_p^n, account for the electric field coupling and controlled voltage sources, V_L^n, account for the magnetic field coupling.

of the type Lp_{ij}, $\boldsymbol{R}$ is a matrix containing the volume cell resistances, V is a vector containing the node potentials (solution), elements of the type ϕ_i, I is a vector containing the branch currents (solution), elements of the type I_i, I_s is a vector containing the current source excitation, and V_s is a vector containing the voltage source excitation. The first row in the equation system in (3) is Kirchoff's current law for each node while the second row satisfy Kirchoff's voltage law for each basic PEEC cell (loop). The use of the MNA method when solving PEEC models is the preferred approach since additional active and passive circuit elements can be added by the use of the corresponding MNA stamp. For a complete derivation of the quasi-static and full-wave PEEC circuit equations using the MNA method, see for example [9].

3 Grid Software

There exist various software for creating grid applications. The choice of method is, for example, dependent on the purpose and performance of the final task and the possibility to put in time and effort in the creation of the grid application. Below follows a short introduction to two technologies.

3.1 Alchemi

Alchemi [10] is a part of the GRIDBUS project [11] and is a .NET-based grid computing framework (grid middleware) that provides the runtime machinery and programming environment required to construct desktop grids and develop grid applications [11]. Alchemi is free and relatively simple to use and a cross-platform support is provided via a

web services interface and an execution model that supports dedicated and non-dedicated (voluntary) execution by grid nodes. It has been designed with the goal of being easy to use and thus more advanced features and performance have been cut. Security feature all programs trying to connect to the manager needs a username and password to an account on the manager. There are three different groups of accounts Executors, Users, and Administrators. Each activity that the manager can perform is accessed with permission.

3.2 Cactus

Cactus [12] originates from the research community where it have been used and developed for many years. One might consider to use Cactus software to perform parallel programming across different architectures using F77, F90, C, and C++. Cactus supports most of the OS architectures on the market today, including Windows. Cactus provides with access to many software technologies for example the Globus Toolkit, HDF5 parallel file I/O, the PETSc scientific library, adaptive mesh refinement, web interfaces, and visualization tools. Cactus is Open Source and the languages C and C++ can be used.

3.3 Globus Toolkit

The Globus Toolkit [13] is an open source toolkit for projects that want to make use of a grid solution. It is not a complete solution, more like a help to get moving in the right direction. Globus security features are divided in to four different parts: Basic security mechanisms, components for credential generation, components for credential management, and components for access control and authorization. Support in setting up security mechanisms in your grid and grid application is provided. The toolkit is for experienced users, and is not a plug-and-play environment like the previous Alchemi.

4 Grid-PEEC

The purpose is to improve the performance of a 3D, quasi-static, frequency domain, PEEC-based EM solver capable of handling nonorthogonal structures. The original code is written in C++ and runs on a Windows environment. This type of code (quasi-static, FD, and nonorthogonal) was chosen since;

- Quasi-static, frequency domain PEEC solvers operate on static partial elements with the multiplication of the phase shift at each frequency thus there is no need for recalculating the elements at each frequency (as for full-wave solvers) which simplifies the task.

- Nonorthogonal partial elements are time consuming to calculate and thus a considerable speed up could be expected. Consider the calculation of nonorthogonal partial inductances using a simple Gauss-Legendre quadrature. In the current code

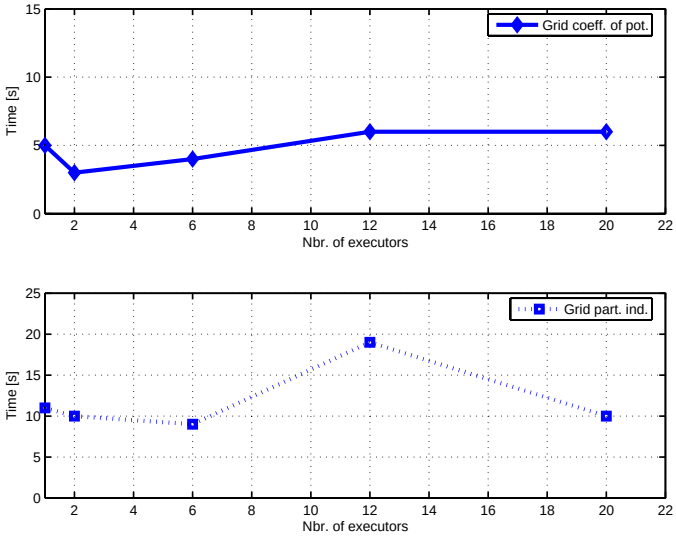

Figure 3: Calculation time for orthogonal partial elements when increasing the number of executors, (top) coefficients of potentials and (bottom) partial inductances.

this takes 13 ms/inductance when using 5 weights for the length and width direction respectively and 2 weights in the thickness direction. For near couplings, 8th order Gauss-Legendre quadrature can be necessary increasing the time to 75 ms/inductance. Coefficients of potentials are somewhat faster to calculate since we assume the charges to reside on the surface of the conductors converting the volume integral from the last term in eq. (2 to a surface integration.

- To solve for each frequency point no history of previous voltages and currents are needed as for time domain solvers thus simplifying the task.

The choice to use Alchemi was based on the usage of the old code written in C++ without major modifications the simplicity to setup and manage the grid application. There are three grid applications created by the grid-PEEC program. The first one is the *Calculation of Coefficients of Potentials*, grid-application two is the *Calculation of Partial Inductances*, and the third is the *Solution of Frequency Domain Problem*. The PEEC program will execute these grid applications one at a time starting with *Calculation of Coefficients of Potentials*, then in turn follows as mentioned above. The PEEC-program creates a thread that creates a grid-application that sends the calculations out on the grid. The thread that started the grid application is in the meantime stopped/paused until its grid-application calculations is carried out. The original PEEC code uses the Matrix TCL Pro 2.12 and complex, linear algebra library. Since these are written in C/C++ and this causes problems when used in a DLL that is used on an Alchemi Grid writing new libraries for matrices and complex numbers in Managed C++ solved this

problem. The modified code works as follows:

1. Manager performs:
   - parsing and meshing,.
   - calculations of $\mathbf{A}$ and $\mathbf{R}$.
   - setup $\mathbf{I}_S$ and $\mathbf{V}$.
   - check how many executors.
2. Partition calculation of coefficients of potentials on the connected executors (fill $\mathbf{P}$). Keep track of non-fill-ins.
3. Partition calculations of partial inductances on the connected executors (fill $\mathbf{L}$). Keep track of non-fill-ins.
4. Solve eq. (3) on the executors. Collect the results.

5 Result

5.1 Test Environment

The test was preformed with different numbers of executors (1, 2, 6, 12 and 20). All of the executors were running on Dell Optiplex GX260, P4-2.0 GHz, 640 Mb RAM, and Gigabit network card. The manager was run on an IBM Thinkpad R50p with a 1.5 GHz Centrino, 512 Mb RAM, and a 100 Mbit/s network card. The executors where all located in the same computer lab and the manager in a nearby office. The bandwidth of the network between the two rooms is 100 Mbit/s. The Grid-PEEC program was run on the same computer as the manager.

5.2 Test Object: Orthogonal $\frac{\lambda}{2}$ dipole

This section shows the results for a $\frac{\lambda}{2}$ dipole discretized using orthogonal cells thus enabling the usage of analytical calculation routines for partial elements. These computations are performed in approximately μs and therefore no speed up can be expected du to the slow connection of computers on the grid. Consider the results for the calculation of partial elements as shown in Fig. 3. It is clear that grid computations are not suitable for these type of structures.

5.3 Test object: Nonorthogonal Transmission Line

This section present results for a simple nonorthogonal transmission line, see Fig. 4. The test object is generic in the sense that another object discretized in the same manner would give the same speed up. The TL is differential fed with a unitary current source and the near- and far- end is terminated using 50 Ω resistances. The TL is discretized

using 200 nodes and the near- and far- end responses are calculated. The near end voltage (magnitude and phase) calculated by the grid-PEEC solver is shown in Fig. 5.

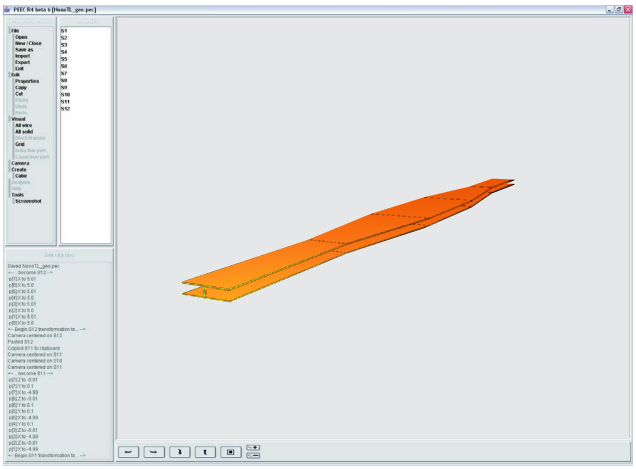

Figure 4: Transmission line with nonorthogonal part.

5.3.1 Partial Element Calculations

The structure requires the calculation of

- 200 self and 19 900 mutual coefficients of potentials (cops) using a 5-5-1 Gauss-Legendre quadrature rule and
- 198 self and 19 503 mutual partial inductances using a 5-5-2 Gauss-Legendre quadrature rule.

The old code calculated the cops in 10 seconds and the partial inductances in 320 seconds. The grid-PEEC calculation times for the partial elements are shown in Fig. 6 for an increasing number of executors. It is clear that the partial element calculation time is not improved by the grid-PEEC application.

5.3.2 Solution of Frequency Domain System

The frequency sweep is performed from 1 MHz to 10 GHz using 1 000 points. The old code performed the 1 000 calculations (solutions) in 65 minutes on the manager computer (IBM-R50). The grid-PEEC execution time for the frequency sweep is shown in Fig. 7 (left) for an increasing number of executors. From the figure, it is clear that the frequency sweep time is clearly improved by the grid-PEEC application. However, five executors

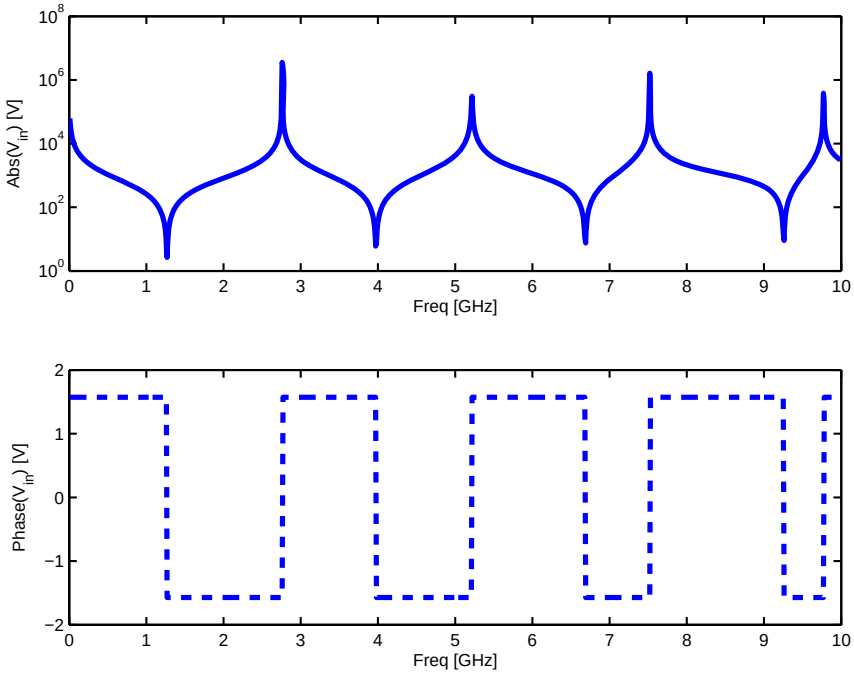

Figure 5: Transmission line input voltage (top-magnitude, bottom-phase).

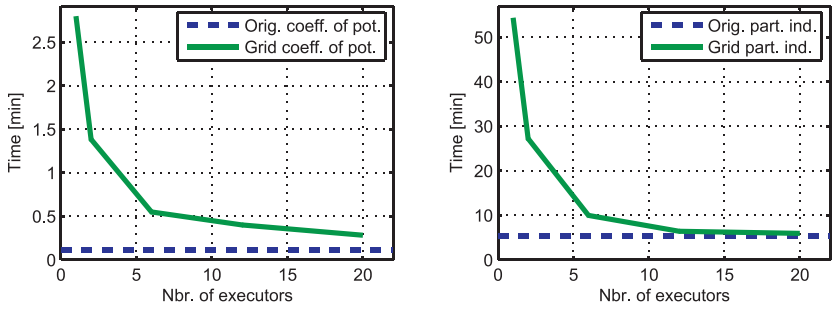

Figure 6: Speed up when increasing the number of executors. (Left) shows the lack of speed up for calculating coefficients of potentials while (right) shows the lack of speed up for calculating partial inductances.

are required to improve the calculations, and by using 20 executors the time is reduced by 78%.

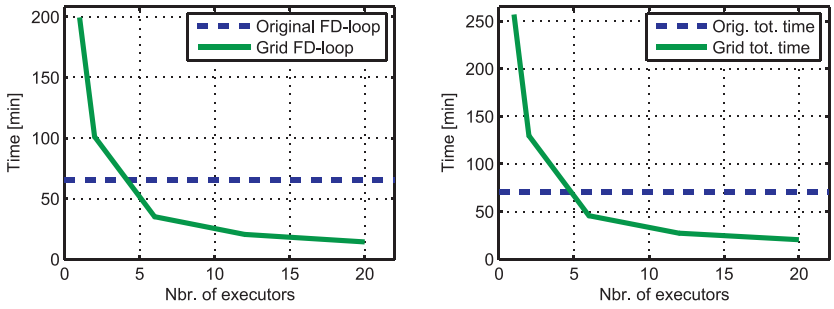

Figure 7: Speed up when increasing the number of executors. (Left) shows the speed up for the repeated frequency domain solution while (right) shows the speed up for the total grid-PEEC solver.

5.3.3 Total Solution time

Even if the grid code does not speed up the partial element calculations, as seen in Fig. 6, the overall solution time is improved due to the dominance of the solution time for the frequency domain circuit equations which are clearly improved.

6 Conclusions & Discussion

From the results presented in Figs. 6 and Fig. 7 it is obvious that the calculations of the partial elements could not be improved with the presented approach. However, the solution time for the frequency domain systems were reduced by 50% by using 6 executors and by 78% by using 20 executors. Looking at the total solver time this were reduced by 46% by the use of 6 executors and by 71% by the use of 20 executors. One problem with this approach was shown to be the case when an executor stopped executing the thread that it was working on. This required matrix fill-in monitoring that possibly had a negative influence on partial element calculation speed up. It is obvious that grid computing on a LAN is not the most suitable for this type of problem even if a considerable speedup is recorded. Therefore, current work involves the modification of the code to run on a parallel cluster for high performance computing [14].

References

[1] A. E. Ruehli, "Inductance calculations in a complex integrated circuit environment", *IBM Journal of Research and Development*, 16(5):470-481, September 1972.

[2] A. E. Ruehli and P. A. Brennan, "Efficient capacitance calculations for three-dimensional multiconductor systems", *IEEE Trans. on Microwave Theory and Techniques*, 21(2):76-82, February 1973.

[3] A. E. Ruehli, "Equivalent circuit models for three-dimensional multiconductor systems", *IEEE Trans. on Microwave Theory and Techniques*, 22(3):216-221, March 1974.

[4] A. E. Ruehli *et al.*, "Nonorthogonal PEEC formulation for time- and frequency-domain modeling". *IEEE Trans. on EMC*, 45(2):167-176, May 2003.

[5] G. Antonini, A. Orlandi, and A. Ruehli "Speed-up of PEEC Method by using Wavelet Transform", in *Proc. of the IEEE Int. Symposium on EMC*", Washington, DC, USA, 2000.

[6] G. Antonini, "The Fast Multipole Method for PEEC Circuit Analysis", in *Proc. of the IEEE Int. Symposium on EMC",* Minneapolis, MN, USA", 2002.

[7] J. Held and D. Johansson, "Optimization of Experimental Computational Electromagnetic Code & Grid Computing for PEEC", Bachelors thesis, Luleå University of Technology, 2005.

[8] C. Ho, A. Ruehli and P. Brennan, "The modified nodal approach to network analysis", *IEEE Trans. on Circuits and Systems*, pages 504–509, June 1975.

[9] J. E. Garrett, "Advancements of the Partial Element Equivalent Circuit Formulation", PhD dissertation, The University of Kentucky, 1997.

[10] Alchemi [.NET Grid Computing Framework] Homepage (2005-05-17). [Online]. Available: http://www.alchemi.net/

[11] Grid Computing and Distributed Systems (GRIDS) Laboratory Homepage (2005-05-17). [Online]. Available: http://www.gridbus.org/

[12] The Cactus Code Server Homepage (2005-05-17). [Online]. Available: http://www.cactuscode.org/

[13] The Globus Alliance Homepage (2005-05-17). [Online]. Available: http://www.globus.org/

[14] HPC2N - High Performance Computing Center North (2006-05-20). [Online]. Available: http://www.hpc2n.umu.se/